



## Uniform asymptotic approximations for accurate modeling of cracks in layered elastic media\*

ANTHONY P. PEIRCE<sup>1</sup> and EDUARD SIEBRITS<sup>2</sup>

<sup>1</sup>*Department of Mathematics, University of British Columbia, Vancouver, BC, Canada (Author for correspondence; e-mail: peirce@math.ubc.ca)*

<sup>2</sup>*Schlumberger, Sugar Land, Texas, USA*

Received 6 January 2000; accepted in revised form 31 January 2001

**Abstract.** We present uniform asymptotic solutions (UAS) for displacement discontinuities (DD) that lie within the middle layer of a three layer elastic medium. The DDs are assumed to be normal to the two parallel interfaces between the elastic media, and solutions will be presented for both 2D and 3D elastic media. Using the Fourier transform (FT) method we construct the leading term in the asymptotic expansion for the spectral coefficient functions for a DD in a three layer medium. Although a closed form solution will require an infinite series solution, we demonstrate how this UAS can be used to construct highly efficient and accurate solutions even in the case in which the DD actually touches the interface. We present an explicit UAS for elements in which the DD fields are assumed to be piecewise constant throughout a line segment in 2D and a rectangular element in 3D. We demonstrate the usefulness of this UAS by providing a number of examples in which the UAS is used to solve problems in which cracks just touch or cross an interface. The accuracy and efficiency of the algorithm is demonstrated and compared with other numerical methods such as the finite element method and the boundary integral method.

**Key words:** Cracks intersecting interfaces, Fourier transforms, layered elastic media, uniform asymptotic solutions.

### 1. Introduction

The solution of fracture problems in layered elastic media is important in a number of applications of the theory of elasticity. For example tabular excavations in rock masses that are layered due to sedimentation can be modeled by planar cracks. Another important application of fracture modeling in layered elastic media occurs in the oil recovery process. In this case it is important to model the evolution of a hydraulically driven fracture as it progresses in a layered rock mass. In the modeling of this process, it is important to be able to solve the boundary value problem for a pressurized crack that intersects a number of layers. The elastic moduli in these problems can differ by at least an order of magnitude from one layer to the next, which can cause severe ‘pinching’ of the crack profile in the stiffer layers. In addition, the models often involve layers of very different thickness ranging from 0.2 m to 200–1000 m. One of the biggest challenges in building models for cracks intersecting layered materials, is to achieve an accurate model of the regions in which the cracks cross or touch an interface. The uniform asymptotic solutions we introduce in this paper have been developed to achieve an efficient and accurate technique to model such situations.

Boundary integral methods (see Crouch and Starfield, 1990) are perhaps the most efficient methods for modeling crack problems in *homogeneous* elastic media. Unfortunately, unlike other methods such as the finite element method, extension to layered materials is not trivial. For bodies that involve just two materials it is possible to obtain closed form solutions for two bonded uniform materials (see Crouch and Starfield, 1990). However, for problems with multiple materials (each of which is uniform), it is necessary to discretize the layer interfaces and to bond the materials within the layers by imposing continuity conditions. This discretization process severely restricts the size of problem that can be solved accurately. Material layering can be modeled trivially using the finite element method, but crack modeling requires that specialized crack elements and mesh refinement be used close to the crack tip. The method we describe, will exploit the layered structure of the rock mass to determine the appropriate numerical Green's function for a multilayered elastic material which comprises a number of layers with different material moduli which are bonded together at interfaces that are all parallel (see Figure 1). The Green's function can then be used to determine the kernel functions for a boundary integral equation that can be used to solve boundary value problems for cavities or cracks that exist within the layered elastic material. Although the method is quite general, in this paper we restrict our discussion to multilayered problems containing cracks that are perpendicular to the layer interfaces.

In order to determine the Green's function, we will apply the FT in one (in 2D) or two (in 3D) directions parallel to the layers in order to reduce the system of partial differential equations to a system of coupled ordinary differential equations. Implicit in the use of the FT is the assumption that we are only looking for solutions whose displacements and stresses decay to zero at infinity. The general solution of the homogeneous ordinary differential equations for a given layer can be determined since any given layer is uniform and therefore has constant coefficients. The general solution in each layer can be expressed in terms of a small number (4 in 2D and 6 in 3D) free constants, which we shall refer to in this paper as spectral coefficients. The appropriate Green's function can then be constructed by stitching together the solutions within each of the layers by applying the conditions that the stresses and displacements are continuous across the layers, while the source term for the Green's function can be derived by specifying the appropriate jump conditions across the pseudo interface at the horizon at which the desired source falls. In order to obtain the spatial form of the Green's function, the FTs are inverted. Using this FT technique, it is possible to determine the Green's function for two bonded half-spaces with different moduli. However, it is not possible to obtain a closed form solution for more than three layers without resorting to an infinite series of image sources (see, for example, Wallace, 1984). The method we describe in this paper is useful for determining numerical Green's functions in an efficient manner. For 3D problems it is perhaps more convenient to use the Hankel transform (or an expansion in terms of Hansen potentials – see Singh, 1970 or Kennet, 1983). The method we describe will apply equally to a formulation in terms of Fourier and Hankel transforms, but for clarity of exposition and to allow the possibility of presenting the method for both 2D and 3D problems within the same framework, we will restrict our discussion to the FT formulation.

The FT method described above for the construction of Green's functions was essentially pioneered by Sneddon (1995). Thompson (1950) introduced the first systematic approach to layered materials. The method described above leads naturally to the so-called stiffness matrix method (see Wardle, 1980), which leads to a system of algebraic equations for the spectral coefficients. A number of formulations of the algebraic equations for layered elastic materials have been developed. Gilbert and Backus (1996) introduced the so-called propagator matrix

method, while Buffler (1961, 1962, 1971) introduced the flexibility matrix method. Many authors (see, for example, Singh, 1970; Wardle, 1980) have dealt with the construction of singular solutions in the frequency domain such as those for an isolated displacement discontinuity (DD) within a layered material that is not close to an interface. The idea is to first subtract off the singular, high wavenumber components, which would correspond to a DD in an infinite elastic medium with the same material properties as those of the elastic layer in which the DD actually falls. Having removed these high frequency components, it is possible to invert the FTs to obtain the residual stress components which need to be added to the infinite space DD in order to take account of the effect of the layering. This process of inversion and integration into discrete elements for the low wavenumber components is typically achieved by numerical integration. However, if the source DD is close to an interface between two of the layers, then the infinite space DD solution only becomes a reasonably good approximation to the singular DD in the layered material for wave numbers  $k = O(1/h)$  where  $h$  is the distance between the DD and the interface. Thus as the DD approaches the interface, i.e., as  $h \rightarrow 0$ , the numerical task of inverting and integrating the residual Fourier coefficients that have significant components for wavenumbers as high as  $k = O(1/h)$  becomes very costly. In this paper we present UASs (in 2D and 3D) that can be used to subtract off the singular components for a point DD that can come arbitrarily close to an interface. These solutions are based on the FT solutions for two pairs of bonded half-planes that are superimposed to construct the leading order asymptotic solution to the problem of a DD in the middle layer of a three layer material. The asymptotic solution is uniformly valid for any location of the DD within the middle layer. Once the singular components due to the UASs have been subtracted off, the residual Fourier coefficients that need to be inverted and integrated numerically only involve very low wavenumbers. Not only do the UASs make it possible to model a problem in which a DD can actually touch an interface, but they also significantly reduce the computational cost because lower order integration and substantially less wavenumber sample points need to be used.

In Section 2 we summarize the governing equations and define the layer geometry. In Section 3 we describe the FT technique to reduce the elastic partial differential equations to systems of ordinary differential equations. In Section 4 we detail the construction of the 2D and 3D UASs in the wavenumber domain. In Section 5 we describe the process of inversion of the 2D and 3D UASs from the wavenumber domain into the spatial domain. In Section 6 we briefly describe the process used to set up the discretized model for a crack in a layered elastic medium. In Section 7 we provide some numerical results to illustrate the accuracy and efficiency of the method based on the UASs. In Section 8 we provide some concluding remarks and discuss some of the applications of this method.

## 2. Governing equations and layer geometry

### 2.1. AN ELASTIC MATERIAL IN 3D

Consider a linear elastic material that occupies a region in 3D space and which is in a state of equilibrium. In this case the stresses  $\sigma_{ij}$  and the strains  $\epsilon_{ij} = \frac{1}{2}(u_{i,j} + u_{j,i})$ , which are defined in terms of the displacement gradients  $u_{i,j} = \partial u_i / \partial x_j$ , at any point within the body are related by:

$$\sigma_{ij} = \lambda \epsilon_{kk} \delta_{ij} + 2G \epsilon_{ij} , \quad (2.1)$$

where  $\lambda$  and  $G$  are Lamé's constants that can be expressed in terms of the Young's modulus  $E$  and Poisson's ratio  $\nu$  of the material by the formulae:  $\lambda = E\nu/[(1 + \nu)(1 - 2\nu)]$  and  $G = E/[2(1 + \nu)]$ . It is convenient to introduce the constants  $a$ ,  $b$ , and  $f$  that are defined by:  $a = \lambda + 2G$ ,  $b = \lambda$ , and  $f = 2G$ .

We assume that the elastic medium is in equilibrium so that the stresses satisfy the equilibrium equations

$$\sigma_{ij,j} + f_i = 0, \quad (2.2)$$

where  $f_i$  are the applied body forces.

It is also useful in this context, in which the layer properties do not change in the  $x$  and  $z$  directions but do vary in the  $y$  direction (see Figure 1), to rewrite the system equations (2.1) and (2.2) in the form of a system in which the  $x$  and  $z$  derivatives have been separated from the  $y$  derivatives:

$$\partial_y T = AT + F, \quad (2.3)$$

where  $T$  represents the vector of stresses and displacements defined by

$$T = [\sigma_{yy}, \sigma_{xy}, \sigma_{yz}, u_y, u_x, u_z]^T,$$

the body force vector is given by  $F = [-f_y, -f_x, -f_z, 0, 0, 0]^T$ , and  $A$  is the differential operator involving only  $x$  and  $z$  derivatives that is defined by:

$$A = \begin{bmatrix} 0 & -\partial_x & -\partial_z & 0 & 0 & 0 \\ -\frac{b}{a}\partial_x & 0 & 0 & 0 & \frac{(b^2 - a^2)}{a}\partial_{xx} - \frac{f}{2}\partial_{zz} & \left(\frac{(b^2 - ab)}{a} - \frac{f}{2}\right)\partial_{xz} \\ -\frac{b}{a}\partial_z & 0 & 0 & 0 & \left(\frac{(b^2 - ab)}{a} - \frac{f}{2}\right)\partial_{xz} & \frac{(b^2 - a^2)}{a}\partial_{zz} - \frac{f}{2}\partial_{xx} \\ \frac{1}{a} & 0 & 0 & 0 & -\frac{b}{a}\partial_x & -\frac{b}{a}\partial_z \\ 0 & \frac{2}{f} & 0 & -\partial_x & 0 & 0 \\ 0 & 0 & \frac{2}{f} & -\partial_z & 0 & 0 \end{bmatrix}. \quad (2.4)$$

## 2.2. GEOMETRY OF THE LAYERED ELASTIC MATERIAL

In this section we introduce the geometry and labeling convention that we will assume for the elastic medium throughout this paper.

We assume that the body is divided into  $N$  layers in which the moduli can be different (see Figure 1). Depending on the problem being considered, the pack of  $N$  layers can either extend to  $\infty$  in both directions or there can be a free surface on the top of the pack of layers,

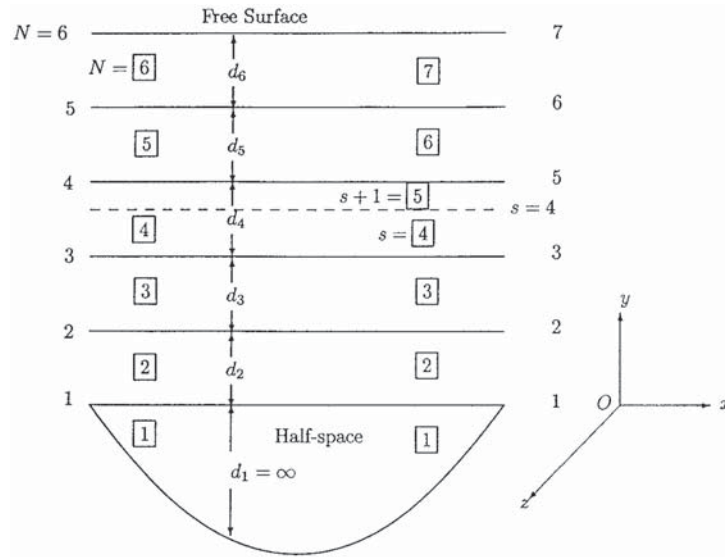


Figure 1. Geometry and labeling of a horizontally layered body.

which rest on an elastic half-space (as is shown in Figure 1). We assign numbers to the layers starting from layer 1 for the bottom half-space and ending with layer number  $N$  for the top layer adjacent to the free surface. These layer indices are represented by the boxed sequence of numbers on the left side of Figure 1. The layer interfaces are numbered in a similar way and the sequence of interface indices for this problem are shown on the extreme left hand side of Figure 1. Observe that the interface at the top of a layer has the same index as the layer itself. The thicknesses of the layers  $d_i$ , which may all be distinct, are also shown in the figure. Similarly, the symbols  $E_i$  and  $\nu_i$  are used to denote the elastic moduli of the  $i$  th layer. We introduce a Cartesian coordinate system  $Oxyz$  in which the  $x$  and  $z$  axes are aligned with the horizontal layers and in which the  $y$  coordinate is measured upwards from the interface between the pack of layers and the bottom half-space (see Figure 1).

Point displacement or force discontinuities can be introduced into the  $N$ -layer elastic medium by specifying appropriate jump conditions in the stress and displacement fields across a horizontal layer having the same  $y$  coordinate as the desired source point. This is achieved by introducing a pseudo interface, which is represented by the dashed line through layer 4 in Figure 1. This process divides layer 4 into two layers for the purposes of this source computation and increases the number of layers by one. For the purpose of the computation the layers are renumbered using the same procedure as before and the layer numbers and interface indices are shown on the right hand side of Figure 1. The symbol  $s$  will be reserved for the  $s$  th layer immediately below the pseudo ‘source’ interface.

### 3. FT solution of the layer equations

There is a vast literature on the application of the FT to singular solutions for elastic media (Sneddon, 1995) and to layered isotropic (Buffler, 1961, 1962; Singh, 1970; Lin, 1989), and even layered transversely isotropic media (Wardle, 1980; Singh, 1986; Lin, 1989; Pan, 1997).

The FT is the fundamental device that we will use in this paper to exploit the horizontal layering of the elastic medium being considered. The fact that the material properties do not vary in the  $x$  and  $z$  directions implies that the FT can be applied to the system of partial differential equations (2.1) and (2.2) to reduce them to a system of ordinary differential equations in the independent variable  $y$  for each of the stress and displacement components in each of the layers (see Appendix A for the definition of the FT used in this paper). Regarding the spatial wavenumber as a parameter, it is possible to obtain the general solution to the system of ordinary differential equations in each of the layers, which in 3D involves six arbitrary constants that need to be determined for each layer.

### 3.1. REDUCTION OF THE LAYER PDES TO A SYSTEM OF ODES

By taking the FT of the system of equations (2.3) we obtain:

$$\partial_y \hat{T} = \hat{A} \hat{T} + \hat{F}, \quad (3.1)$$

where  $\hat{A}$  is defined to be:

$$\hat{A} = \begin{bmatrix} 0 & -k & 0 & 0 & 0 & 0 \\ \frac{b}{a}k & 0 & 0 & \frac{(a^2 - b^2)}{a}k^2 & 0 & 0 \\ \frac{1}{a} & 0 & 0 & -\frac{b}{a}k & 0 & 0 \\ 0 & \frac{2}{f} & k & 0 & 0 & 0 \\ 0 & 0 & 0 & 0 & 0 & \frac{f}{2}k \\ 0 & 0 & 0 & 0 & \frac{2}{f} & 0 \end{bmatrix} \quad (3.2)$$

and  $k = (m^2 + n^2)^{\frac{1}{2}}$  and the elements of  $\hat{T}$  and  $\hat{F}$  have been arranged as follows

$$\hat{T} = [\hat{\sigma}_{yy}, \hat{\tau}_s, \hat{u}_y, \hat{u}_s, \hat{\tau}_t, \hat{u}_t]^T \quad \text{and} \quad \hat{F} = [-\hat{f}_y, -\hat{f}_s, 0, 0, -\hat{f}_t, 0]^T.$$

Here we have followed Wardle (1980) by defining the displacement and stress components of  $\hat{T}$  to be:

$$\hat{u}_s = -i(m\hat{u}_x + n\hat{u}_z)/k, \quad \hat{u}_t = -i(n\hat{u}_x - m\hat{u}_z)/k \quad (3.3)$$

and

$$\hat{\tau}_s = -i(m\hat{\sigma}_{xy} + n\hat{\sigma}_{yz})/k, \quad \hat{\tau}_t = -i(n\hat{\sigma}_{xy} - m\hat{\sigma}_{yz})/k. \quad (3.4)$$

We observe that unknowns involving  $\hat{\sigma}_{yy}$ ,  $\hat{\tau}_s$ ,  $\hat{u}_y$  and  $\hat{u}_s$  (the  $s$  subsystem) are completely decoupled from the unknown involving  $\hat{\tau}_t$  and  $\hat{u}_t$  (the  $t$  subsystem). The  $s$  subsystem is sufficient to determine boundary value problems for 2D plane strain, while the autonomous  $t$  subsystem is the only additional part that needs to be added to the plane strain equations in order to determine boundary value problems in 3D. We notice that by setting either  $m = 0$  (or  $n = 0$ ) we obtain the corresponding plane strain equations with the out of plane direction being the  $x$  (respectively the  $z$ ) direction. A similar decoupling of the spectral ODEs also occurs if the Hankel transformation is applied to the layered elasticity problem (see, for example, Singh, 1970; Kennet, 1983).

### 3.2. EXACT SOLUTION TO THE LAYER ODEs AND SPECTRAL COEFFICIENTS

Considering the wavenumber  $k$  as a parameter, we can now determine the solution to the system of ODEs (3.1), which can be expressed in terms of the solutions for the  $s$ -subsystem and the  $t$ -subsystem as follows (see Wardle, 1980):

$$\begin{bmatrix} T_s \\ T_t \end{bmatrix} = \begin{bmatrix} Z_s & 0 \\ 0 & Z_t \end{bmatrix} \begin{bmatrix} A_s \\ A_t \end{bmatrix}, \quad (3.5)$$

where

$$T_s = [\hat{\sigma}_{yy}^l/k, \hat{\tau}_s^l/k, \hat{u}_y^l, \hat{u}_s^l]^T, \quad A_s = [A_1, A_2, A_3, A_4]^T,$$

$$T_t = [\hat{\tau}_t^l/k, \hat{u}_t^l]^T, \quad A_t = [A_5, A_6]^T,$$

$$Z_s = \begin{bmatrix} -f e^{-ky} & (l_4 - fky)e^{-ky} & f e^{ky} & (l_4 + fky)e^{ky} \\ -f e^{-ky} & (l_5 - fky)e^{-ky} & -f e^{ky} & -(l_5 + fky)e^{ky} \\ e^{-ky} & kye^{-ky} & e^{ky} & kye^{ky} \\ e^{-ky} & (ky - l_2)e^{-ky} & -e^{ky} & -(ky + l_2)e^{ky} \end{bmatrix}$$

and

$$Z_t = \begin{bmatrix} -\frac{f}{2}e^{-ky} & \frac{f}{2}e^{ky} \\ e^{-ky} & e^{ky} \end{bmatrix}.$$

The constants  $l_j$  in (3.5) are defined as follows:

$$l_2 = \frac{\lambda + 3G}{\lambda + G}, \quad l_4 = \frac{2G^2}{\lambda + G}, \quad l_5 = \frac{2G(\lambda + 2G)}{\lambda + G} \quad (3.6)$$

and the following relationships between the above constants are useful:

$$fl_2 = l_5 + l_4, \quad f = l_5 - l_4. \quad (3.7)$$

It is important to note that the spectral coefficients, required to define the primary variables, can be expressed entirely in terms of the single wavenumber parameter  $k = \sqrt{m^2 + n^2}$ . This property can be exploited to reduce the FT inversion problem from one which involves sampling the integrand at points throughout the  $(m, n)$  plane to what amounts to a 1D sampling

of the wavenumber parameter  $k$ . The unknown coefficients  $A_j(k)$  in (3.5) depend on the parameter  $k$ , and we will refer to them as the spectral coefficients throughout this paper. Once the spectral coefficients in any one layer are known, it is then possible using (3.5) to determine the stresses and displacements at any desired point within that layer.

It can be shown (Kennet, 1983) that a normal point vertical DD located at  $y_s$  with a displacement jump  $\Delta u$  in the  $z$  direction can be represented by traction discontinuities across the plane  $y = y_s$  of the following form:

$$[\hat{T}(y_s)] = \begin{bmatrix} 0 \\ \frac{\Delta u(b^2 - a^2)}{a} \\ \frac{\Delta u b}{a} \\ 0 \\ 0 \\ 0 \end{bmatrix} + \frac{m^2}{(m^2 + n^2)} \begin{bmatrix} 0 \\ \Delta u(a - b) \\ 0 \\ 0 \\ 0 \end{bmatrix} + \frac{mn}{(m^2 + n^2)} \begin{bmatrix} 0 \\ 0 \\ 0 \\ 0 \\ \Delta u(a - b) \\ 0 \end{bmatrix}. \quad (3.8)$$

The first forcing vector on the right-hand side of (3.8) is precisely the same one that appears in plane strain problems and only acts on the  $s$ -system and we will refer to the solutions obtained using this forcing as the  $Ps$  solution. The second forcing vector is in the form of a forcing on the  $s$ -subsystem and we will refer to this as the ancillary  $s$  solution which we will denote by the  $As$  solution. The third vector is in the form of a forcing on the  $t$ -subsystem and we refer to this ancillary solution as the  $At$  solution. Because the dependence on  $m$  and  $n$  can be factored out of each of these forcing vectors, we can determine the solution for the forcing vectors without the factors involving  $m$  and  $n$ , and then we can multiply these solutions by the appropriate functions of  $m$  and  $n$  in order to get the required solution for any given wavenumber pair  $(m, n)$ .

In order to model vertical fractures that run perpendicular to the layers, it is necessary to derive an expression for the stress normal to the fracture surface. In the coordinate systems defined in Figure 1 it is necessary to determine the stress component  $\hat{\sigma}_{zz}$ , which can be defined in terms of the spectral coefficients as follows:

$$k\hat{\sigma}_{zz} = fn^2A_1e^{-ky} + (-l_6n^2 - l_7m^2 + fn^2ky)A_2e^{-ky} - fmnA_5e^{-ky} - fn^2A_3e^{ky} + (-l_6n^2 - l_7m^2 - fn^2ky)A_4e^{ky} - fmnA_6e^{ky}, \quad (3.9)$$

where we have defined the new constants  $l_6 = 2G(2\lambda + 3G)/(\lambda + G)$  and  $l_7 = 2\lambda G/(\lambda + G)$ .

### 3.2.1. Inversion of the FTs

Once the values of the spectral coefficients  $A_j(k)$  in each layer have been determined and the FT of the displacements  $\hat{u}_i(k)$  and stresses  $\hat{\sigma}_{ij}(k)$  within each layer have been determined, then the displacements and stresses within each layer can be determined by applying formula (A.2) for the inversion of the FT. We will discuss the process of inverting the double FT by converting the double integral into polar coordinates and expressing the double integrals in terms of a single Hankel transform using an integral representation of the Bessel function.

### 3.2.2. Asymptotic behavior of spectra and the effect on spatial solutions

For a layer in which  $y$  is positive, we observe from (3.5) that in order for the stresses and displacements to remain finite, the spectral coefficients  $A_3(k)$  and  $A_4(k)$  must tend to zero as  $k \rightarrow \infty$  more rapidly than  $e^{ky}$ . For large  $y$  (i.e., in the far-field limit) the behavior of the solution is determined by the value of the spectral coefficients as  $k \rightarrow 0$ , while the near field  $y \rightarrow 0$  behavior will be determined by the values of the spectral coefficients  $A_j(k)$  as  $k \rightarrow \infty$ .

## 3.3. THE NUMERICAL PROCEDURE TO SOLVE BOUNDARY VALUE PROBLEMS

Three different methods have been developed to solve the system of algebraic equations for the spectral coefficients  $A_j(k)$ , namely the stiffness matrix method (see Wardle, 1980; Buffler, 1971), the propagator matrix method (see Gilbert, 1966), and the flexibility matrix method (see Buffler, 1971 or Linkov, 1991 and for a more recent improvement Peirce, 2001), that can be used to determine the solution to the coupled system of algebraic equations that needs to be solved in order to determine the spectral coefficients  $A_j(k)$ .

All these methods rely on a fairly simple idea that is common to all techniques for solving problems in layered elastic media. We first establish the equations that determine the stiffness properties of each of the layers in terms of the degrees of freedom of the model. For example, the degrees of freedom for a finite element, finite difference, or boundary element model will be the unknown nodal displacements at the mesh points of the numerical model. For the spectral methods that we use in this paper, the degrees of freedom in the model are represented by the unknown constants, which we call spectral coefficients, that are parameterized by the wavenumber  $k$ . Once we have established equations for the stresses and displacements within each of the layers in terms of the internal degrees of freedom, we stitch all the layers involved in the problem together at their common interfaces by imposing conditions of continuity in displacements and tractions across the interfaces. Discontinuous sources (such as force discontinuities or DDs) can be represented by introducing the appropriate jump conditions across pseudo-interfaces introduced for this purpose. Finally, the whole mechanical problem is completed into a well-posed system of algebraic equations by introducing the appropriate conditions at the boundaries of the pack of layers, e.g., specified tractions, specified displacements, or a complementary combination of tractions and displacements.

## 4. UASs in the wavenumber domain

In the case of a layered material with multiple layers it is not possible to obtain a simple closed-form solution for the spectral coefficients and therefore for the stresses and displacements due to a DD for example. Indeed, for a problem that has three or more layers and two or more

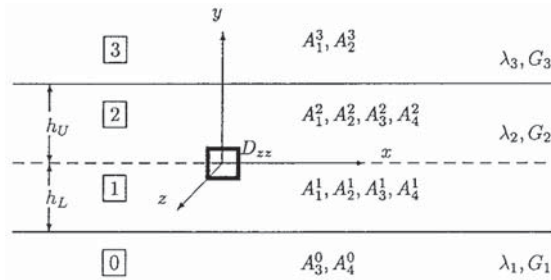


Figure 2. A vertical DD in the middle layer of three bonded elastic layers.

interfaces, the analytic solutions will involve an infinite series of image DDs that are required to impose the appropriate boundary conditions on the interfaces. Thus for a more complex problem, one inevitably has to resort to a numerical solution of the system of algebraic equations for the spectral coefficients and then a numerical inversion. This numerical inversion process, as we will see later in this paper, is essentially equivalent to inverting a Hankel transform. The situation is exacerbated by the presence of highly singular sources in the problem that tend to increase the high frequency content of the spectral coefficients. Indeed, the only feasible way to obtain any sort of numerical inversion in the presence of a concentrated DD, is to first subtract off the singular DD coefficients for a DD in an infinite medium and to then invert the remaining low frequency components using numerical integration (see, for example, Wardle, 1980). However, for problems in which the DD comes very close to an interface, which occurs when modeling a crack touching or intersecting an interface, the asymptotic solution in the limit  $k \rightarrow \infty$  provided by a DD in an infinite medium no longer removes all the high frequency components that prove to be troublesome for numerical integration. If the DD is a small but finite distance from the interface, then *eventually* as  $k \rightarrow \infty$ , the spectral coefficients will tend to the infinite space values. However, if the source DD is really close to the interface, the actual spectral coefficients will be significantly different from the infinite space DD solution for wavenumbers up to  $k = O(h^{-1})$ , where  $h$  is the distance between the source DD and the interface. For this reason we derive a uniform asymptotic approximation to the solution for a vertical DD which is in the middle layer of a three layer medium. This asymptotic approximation, which is valid for large  $k$ , allows us to significantly reduce the range of wavenumbers that need to be calculated – in some cases by two orders of magnitude. But perhaps more importantly it substantially reduces the high frequency content of the spatial influences that need to be integrated numerically in order to obtain an integrated Green's function – this becomes particularly important when trying to arrive at Green's functions for elements that come into contact with the interface between two materials.

#### 4.1. UAS FOR THREE ELASTIC LAYERS

A typical situation encountered when modeling a crack which intersects a number of layers will involve a DD element that finds itself sandwiched between two interfaces. These interfaces separate the layer, in which the DD element falls, from the 'outside world'. The outside world might comprise two or more distinct layers. The first step in finding useful asymptotic solutions would be to determine the solution for a DD element that falls in the middle layer of three elastic layers, i.e., within a layer that is sandwiched between two bonded elastic half-planes. As mentioned earlier, the solution to this problem will involve an infinite series of

image DDs that are distributed about an infinite periodic sequence of image interfaces that are located further and further away from the source as the terms of the series progress (see, for example, Wallace, 1984). These image DDs will result in features that alter the spectral coefficients that decay on a length scale  $e^{-2kH}$ , where  $H$  is the distance from the image to the original source DD. Thus the effects of the remote DD will die very rapidly, leaving spectral coefficients whose behavior is dominated by the source and the nearest images. In this section we use the exact solutions for two bonded half-planes to derive the uniformly valid leading order asymptotic approximation to the spectral coefficients for the three layer problem. These asymptotic spectral coefficients can be used to eliminate the high wavenumber components from the spectral coefficients. Since only the remaining low wavenumber components need to be inverted, this procedure significantly reduces the computational cost of numerical inversion and integrated kernel evaluation. In the performance tests presented below we will see that the UAS makes it possible to efficiently determine the effect of a single DD element that touches two interfaces simultaneously.

Consider a three layer elastic medium comprising two half-planes that are bonded to a finite strip with the moduli and spectral coefficients defined as shown in Figure 2. If the vertical DD falls in the region where  $h_L \ll h_U$ , the three layer solution will tend, for large  $k$  values, to the solution for a vertical DD in the upper part of two bonded half-planes, while if the DD falls in the region where  $h_L \gg h_U$ , the three layer solution will tend, for large  $k$  values, to the solution for a vertical DD in the lower part of two bonded half-planes. If on the other hand, the DD is not much closer to one interface than the other so that  $h_L \sim h_U$ , then as  $k \rightarrow \infty$  the ultimate asymptotic solution is the solution for a vertical DD in an infinite medium to which both the upper and lower solutions tend. Thus we have a typical situation that occurs in asymptotic analysis (see, for example, Bender, 1978), in which two different asymptotic solutions are valid in different regions but they are both valid in a finite overlap region that they both share. In this case it is possible to obtain an asymptotic approximation that is uniformly valid over the three regions by superimposing the two asymptotic solutions and subtracting the solution in the match region:

$$A_j^{l,\mu}(k) \stackrel{k \rightarrow \infty}{\sim} A_j^{l,U}(k) + A_j^{l,L}(k) - A_j^{l,\infty}(k), \quad (4.1)$$

where  $A_j^{l,\mu}(k)$  is used to represent the uniformly valid asymptotic solution,  $A_j^{l,U}(k)$  represents the corresponding bonded half-plane spectral coefficient in which the interface is above the source DD (i.e., for which  $\lambda_2 = \lambda_1$  and  $G_2 = G_1$  so that the lower interface in Figure 2 ceases to have physical significance),  $A_j^{l,L}(k)$  represents the corresponding bonded half-plane spectral coefficient in which the interface is below the source DD (i.e., for which  $\lambda_2 = \lambda_3$  and  $G_2 = G_3$  so that the upper interface in Figure 2 ceases to have physical significance), and  $A_j^{l,\infty}(k)$  represents the spectral coefficient for a point vertical DD in an infinite medium with material properties  $\lambda_2$  for the middle layer.

The unknown asymptotic spectral coefficients  $A_j^{l,Ps\mu}(k)$  that are calculated by substituting the expressions for  $A_j^{l,PsU}(k)$ ,  $A_j^{l,PsL}(k)$ , and  $A_j^{l,Ps\infty}(k)$  into (4.1) are given as follows:

$$\begin{aligned}
A_1^{3,Ps\mu} &= g_1^{PL}(k) + g_0^{PU}(k), & A_2^{3,Ps\mu} &= g_2^{PL}(k) + c_0^U, \\
A_1^{2,Ps\mu} &= g_1^{PL}(k) - c_3, & A_2^{2,Ps\mu} &= g_2^{PL}(k) + c_4, \\
A_3^{2,Ps\mu} &= g_1^{PU}(k), & A_4^{2,Ps\mu} &= g_2^{PU}(k), \\
A_1^{1,Ps\mu} &= g_1^{PL}(k), & A_2^{1,Ps\mu} &= g_2^{PL}(k), \\
A_3^{1,Ps\mu} &= g_1^{PU}(k) + c_3, & A_4^{1,Ps\mu} &= g_2^{PU}(k) + c_4, \\
A_3^{0,Ps\mu} &= g_1^{PU}(k) + g_0^L(k), & A_4^{0,Ps\mu} &= g_2^{PU}(k) + c_0^L.
\end{aligned} \tag{4.2}$$

Here

$$\begin{aligned}
g_0^{PL}(k) &= g_0^P(k; \epsilon_L, \delta_L, \rho, h_L), & g_0^{PU}(k) &= -g_0^P(k; \epsilon_U, \delta_U, \rho, h_U), \\
g_1^{PL}(k) &= g_1^P(k; \epsilon_L, \delta_L, \rho, h_L), & g_1^{PU}(k) &= -g_1^P(k; \epsilon_U, \delta_U, \rho, h_U), \\
g_2^{PL}(k) &= g_2^P(k; \epsilon_L, \delta_L, \rho, h_L), & g_2^{PU}(k) &= g_2^P(k; \epsilon_U, \delta_U, \rho, h_U),
\end{aligned}$$

and where functions  $g_j^P(k; \epsilon, \delta, \rho, h)$  are defined as follows:

$$g_0^P(k; \epsilon, \delta, \rho, h) = \{\alpha_0^0 + \alpha_1^0 \cdot (kh)\}, \tag{4.3}$$

$$g_1^P(k; \epsilon, \delta, \rho, h) = \{\alpha_0^1 + \alpha_1^1 \cdot (kh) + \alpha_2^1 \cdot (kh)^2\}e^{-2kh}, \tag{4.4}$$

$$g_2^P(k; \epsilon, \delta, \rho, h) = \{\alpha_0^2 + \alpha_1^2 \cdot (kh)\}e^{-2kh}, \tag{4.5}$$

and the constants  $\alpha_j^i$  and  $c_j$  are defined as follows:

$$\begin{aligned}
\alpha_0^0 &= -\frac{3\epsilon(1-\epsilon) + (\delta + 3\epsilon)\rho + (1+\epsilon)\delta\rho^2}{(3\epsilon + \epsilon^2 + (1+\epsilon)\rho\delta)(1 + 3\epsilon + (1+\epsilon)\rho)}, \\
\alpha_1^0 &= \frac{2\epsilon\{(1-\epsilon) + (1-\delta)\rho\}}{(3\epsilon + \epsilon^2 + (1+\epsilon)\rho\delta)(1 + 3\epsilon + (1+\epsilon)\rho)}, \\
\alpha_0^1 &= -\frac{12\epsilon(1-\epsilon) + (15\epsilon - 16\epsilon^2 - 3\epsilon^3 + 4\delta)\rho + (3\epsilon - 4\epsilon^2 - \epsilon^3 - 3\epsilon^2\delta + 5\delta)\rho^2 + (1-\epsilon^2)\delta\rho^3}{2(2+\rho)(3\epsilon + \epsilon^2 + (1+\epsilon)\rho\delta)(1 + 3\epsilon + (1+\epsilon)\rho)}, \\
\alpha_1^1 &= -\frac{(1-\epsilon)(1+\rho)\rho}{(2+\rho)(1 + 3\epsilon + (1+\epsilon)\rho)}, \\
\alpha_2^1 &= \frac{(1-\epsilon)(1+\rho)^2}{(2+\rho)(1 + 3\epsilon + (1+\epsilon)\rho)}, \\
\alpha_0^2 &= -\frac{3}{2} \frac{(1-\epsilon)(1+\rho)^2}{(2+\rho)(1 + 3\epsilon + (1+\epsilon)\rho)}, \\
\alpha_1^2 &= \frac{(1-\epsilon)(1+\rho)^2}{(2+\rho)(1 + 3\epsilon + (1+\epsilon)\rho)}, \\
c_0 &= -\frac{(\epsilon + \delta\rho)}{(3\epsilon + \epsilon^2 + (1+\epsilon)\rho\delta)},
\end{aligned} \tag{4.6}$$

$$c_3 = -\frac{\rho}{2(2 + \rho)},$$

$$c_4 = -\frac{1 + \rho}{2(2 + \rho)}.$$

The constants  $\epsilon_L$ ,  $\delta_L$ ,  $\epsilon_U$ ,  $\delta_U$ , and  $\rho$  are defined as follows:

$$\epsilon_L = \frac{G_1}{G_2} \quad \delta_L = \frac{\lambda_1}{\lambda_2} \quad \epsilon_U = \frac{G_3}{G_2}, \quad \delta_U = \frac{\lambda_3}{\lambda_2}, \quad \rho = \frac{\lambda_2}{G_2}.$$

The uniform asymptotic spectral coefficients  $A_j^{l,As\mu}(k)$  that are calculated by substituting  $A_j^{l,AsU}(k)$ ,  $A_j^{AsL}(k)$ , and  $A_j^{l,As\infty}(k)$  into (4.1) are given as follows:

$$\begin{aligned} A_1^{3,As\mu} &= g_1^{AL}(k) + g_0^{AU}(k), & A_2^{3,As\mu} &= g_2^{AL}(k) - c_0^U, \\ A_1^{2,As\mu} &= g_1^{AL}(k), & A_2^{2,As\mu} &= g_2^{AL}(k) - c_4, \\ A_3^{2,As\mu} &= g_1^{AU}(k), & A_4^{2,As\mu} &= g_2^{AU}(k), \\ A_1^{1,As\mu} &= g_1^{AL}(k), & A_2^{1,As\mu} &= g_2^{AL}(k), \\ A_3^{1,As\mu} &= g_1^{AU}(k), & A_4^{1,As\mu} &= g_2^{AU}(k) - c_4, \\ A_3^{0,As\mu} &= g_1^{AU}(k) + g_0^{AL}(k), & A_4^{0,As\mu} &= g_2^{AU}(k) - c_0^L, \end{aligned} \tag{4.7}$$

where

$$\begin{aligned} g_0^{AL}(k) &= g_0^A(k; \epsilon_L, \delta_L, \rho, h_L), & g_0^{AU}(k) &= -g_0^A(k; \epsilon_U, \delta_U, \rho, h_U), \\ g_1^{AL}(k) &= g_1^A(k; \epsilon_L, \delta_L, \rho, h_L), & g_1^{AU}(k) &= -g_1^A(k; \epsilon_U, \delta_U, \rho, h_U), \\ g_2^{AL}(k) &= g_2^A(k; \epsilon_L, \delta_L, \rho, h_L), & g_2^{AU}(k) &= g_2^A(k; \epsilon_U, \delta_U, \rho, h_U), \end{aligned}$$

where the functions  $g_j^A(k; \epsilon, \delta, \rho, h)$  are defined as follows:

$$g_0^A(k; \epsilon, \delta, \rho, h) = \{\beta_0^0 + \beta_1^0 \cdot (kh)\}, \tag{4.8}$$

$$g_1^A(k; \epsilon, \delta, \rho, h) = \{\beta_0^1 + \beta_2^1 \cdot (kh)\}e^{-2kh}, \tag{4.9}$$

$$g_2^A(k; \epsilon, \delta, \rho, h) = \{\beta_0^2 + \beta_1^2 \cdot (kh)\}e^{-2kh}, \tag{4.10}$$

and the constants  $c_j$  were defined in (4.6) and the  $\beta_j^i$  are defined as follows:

$$\beta_0^0 = \frac{3\epsilon(1 - \epsilon) + (\delta - \epsilon^2)\rho}{(3\epsilon + \epsilon^2 + (1 + \epsilon)\delta\rho)(1 + 3\epsilon + (1 + \epsilon)\rho)},$$

$$\beta_1^0 = \frac{2\epsilon\{(\epsilon - 1) + (\delta - 1)\rho\}}{(3\epsilon + \epsilon^2 + (1 + \epsilon)\delta)(1 + 3\epsilon + (1 + \epsilon)\rho)},$$

$$\beta_0^1 = \frac{-(3\epsilon^2 - 3\epsilon + (\epsilon^2 - \delta)\rho)}{(3\epsilon + \epsilon^2 + (1 + \epsilon)\delta\rho)(1 + 3\epsilon + (1 + \epsilon)\rho)},$$

$$\begin{aligned}\beta_2^1 &= \frac{(\epsilon - 1)(1 + \rho)^2}{(2 + \rho)(1 + 3\epsilon + (1 + \epsilon)\rho)}, \\ \beta_0^2 &= \frac{(1 - \epsilon)(1 + \rho)(3 + \rho)}{2(2 + \rho)(1 + 3\epsilon + (1 + \epsilon)\rho)}, \\ \beta_1^2 &= \frac{(\epsilon - 1)(1 + \rho)^2}{(2 + \rho)(1 + 3\epsilon + (1 + \epsilon)\rho)}.\end{aligned}\tag{4.11}$$

The uniform asymptotic spectral coefficients  $A_j^{l,At\mu}(k)$  that are calculated by substituting  $A^{l,AtU}j(k)$ ,  $A^{l,AtL}j(k)$ , and  $A^{l,At\infty}j(k)$  into (4.1) are given as follows:

$$\begin{aligned}A_5^{3,At\mu} &= -\{\gamma_1^L e^{-2kh_L} + \gamma_0^U\}, \quad A_6^{3,At\mu} = 0, \\ A_5^{2,At\mu} &= -\{\gamma_1^L e^{-2kh_L} + 1\}, \quad A_6^{2,At\mu} = -\gamma_1^U e^{-2kh_U}, \\ A_5^{1,At\mu} &= -\gamma_1^L e^{-2kh_L}, \quad A_6^{1,At\mu} = -\{\gamma_1^U e^{-2kh_U} + 1\}, \\ A_5^{0,At\mu} &= 0, \quad A_6^{0,At\mu} = -\{\gamma_0^U + \gamma_1^L e^{-2kh_U}\},\end{aligned}\tag{4.12}$$

where  $\gamma_0 = 2/(1 + \epsilon)$  and  $\gamma_1 = (1 - \epsilon)/(1 + \epsilon)$  and  $\gamma_0^L$ ,  $\gamma_1^L$  and  $\gamma_0^U$ ,  $\gamma_1^U$  are obtained by using the values of  $\epsilon_L$  and  $\epsilon_U$  respectively.

## 5. Inversion of the UAS

In this section we discuss the process of inversion of the FTs of the influences as well as the construction of integrated kernels. In order to make it possible to use the spectral method to determine the spatial influences of the singular case in which a crack intersects the interface between two layers, it is necessary to first subtract off the uniform asymptotic spectral coefficients  $A_j^{l,\mu}(k)$  derived in Section 4.1 from the numerical spectral coefficients  $A_j^l(k)$ . We then obtain a set of low frequency components  $A_j^{l,\mathcal{L}}(k)$  that are used in the numerical inversion process, i.e.,

$$A_j^{l,\mathcal{L}}(k) = A_j^l(k) - A_j^{l,\mu}(k).\tag{5.1}$$

Since  $A_j^l(k) \xrightarrow{k \rightarrow \infty} A_j^{l,\mu}(k)$ , it follows that  $A_j^{l,\mathcal{L}}(k) \xrightarrow{k \rightarrow \infty} 0$ . If the uniform asymptotic approximation closely mimics the true solution, then  $A_j^{l,\mathcal{L}}(k)$  will only be non-zero for relatively low frequencies. After subtracting off the asymptotic solution, the remaining spectral coefficients  $A_j^{l,\mathcal{L}}(k)$  that need to be inverted contain only relatively low frequency components. As a result, it is possible to invert the low frequency spectra  $A_j^{l,\mathcal{L}}(k)$  very efficiently using numerical integration. The high frequency components, that are associated with the UAS  $A_j^{l,\mu}(k)$ , cannot be inverted numerically. However, these uniform special coefficients can be inverted analytically to yield approximate spatial stress and displacement components due to a point vertical DD in a three layer material.

The point kernels must be multiplied by the appropriate basis functions to obtain the desired elemental DD influences. In this paper we shall only consider the case of piecewise constant basis functions, but any of the standard DD discretizations can be obtained for

multilayered media using the spectral method by implementing the appropriate choice of basis functions. In order to complete the process, the low frequency components also need to be integrated against the appropriate basis functions. Since we do not have an explicit expression for the low frequency spectral components that have been inverted numerically, it is not possible to obtain an analytic expression for the integrated low frequency components. The spatial functions associated with these low frequency spectra are smooth functions since they only involve low frequency Fourier modes all of which are smoothly varying functions in space. It is therefore possible to integrate the contribution of these low frequency spectral components very accurately with a low order Gauss integration scheme in order to determine a set of integrated influence coefficients.

If the  $l$ -th layer is adjacent to, or contains, the vertical DD then it is necessary to subtract off the high frequency components before the inversion process. In this case in order to obtain the stress components, we superimpose the low frequency stress components  $\sigma_j^{l,\mathcal{L}}(k)$  that are associated with the spectral coefficients  $A_j^{l,\mathcal{L}}(k)$ , and the singular stress components  $\sigma_{ij}^{l,\mu}$  due to the uniform asymptotic spectral coefficients  $A_j^{l,\mu}(k)$ , i.e.,

$$\sigma_{ij}^l = \sigma_{ij}^{l,\mathcal{L}} + \sigma_{ij}^{l,\mu}.$$

A similar procedure can be followed to obtain the displacement components due to a vertical DD in a multilayered elastic medium, i.e.,

$$u_i^l = u_i^{l,\mathcal{L}} + u_i^{l,\mu}.$$

If the  $l$ -th layer is *not* adjacent to or *does not* contain the vertical DD then it is not necessary to subtract off the high frequency components before the inversion process. In this case the stresses and displacement components can be obtained by direct numerical inversion.

### 5.1. INVERSION OF THE 2D KERNELS

The FT of the horizontal stress component  $\widehat{\sigma}_{xx}^\mu$  due to a point vertical DD of unit strength located a distance  $\eta$  from the center of the sending element (see Figure C.1) can be expressed in the form:

$$\frac{\widehat{\sigma}_{xx}^\mu}{k} = f A_1^\mu(k) e^{-ky'} + (fky' - l_6) A_2^\mu(k) e^{-ky'} - f A_3^\mu(k) e^{ky'} - (fky' + l_6) A_4^\mu(k) e^{ky'}, \quad (5.2)$$

where the spectral coefficients  $A_j^\mu(k)$  are those for the uniform asymptotic approximation defined in (4.2). The detailed coefficients  $A_j^\mu(k)$  and constants  $f$  and  $l_6$  vary depending on which of the four layers, indicated in Figure 2, the receiving point falls in.

The expressions for the spectral coefficients given in (4.2) involve products of powers of  $k$  and exponentials of the form  $e^{-|k|\mathcal{Y}}$ , where  $\mathcal{Y}$  is some function of  $y'$  that will be defined below. As a result the inversion of the point DD influences involves evaluating integrals of the form:

$$\begin{aligned} I_p(x'y') &= \frac{1}{2\pi} \int_{-\infty}^{\infty} e^{-kx'} |k|^p e^{-|k|\mathcal{Y}} dk \\ &= \frac{1}{\pi} \int_0^{\infty} k^p e^{-k\mathcal{Y}} \cos(kx') dk \end{aligned}$$

$$= \frac{1}{\pi} \mathcal{L}(k^p \cos(kx'), k, \mathcal{Y}) .$$

Here  $\mathcal{L}(k^p \cos(kx'), k, \mathcal{Y})$  represents the Laplace transform of  $k^p \cos(kx')$  with respect to  $k$  evaluated at the value of the transform variable  $\mathcal{Y}$ . Depending on the location of the receiving point and the particular term being considered, the Laplace transform variable  $\mathcal{Y}$  can take on the following values  $\mathcal{Y} = |y'|$ ,  $2h_L + y'$ , or  $2h_U - y'$ , representing terms associated with the point DD, the lower image of the point DD, and the upper image of the point DD, respectively.

The inversion process for the 3D kernels follows a similar procedure involving Hankel transforms which is outlined in Appendix B.

## 6. The numerical procedure to solve crack problems

The pressurized crack problem is conveniently expressed (Crouch and Starfield, 1990) in the form of an integral equation:

$$\int_{R(t)} C(x, y; \xi, \eta) w(\xi, \eta, t) d\xi d\eta = p(x, y, t) .$$

Here  $w$  is the unknown width (DD) profile within the crack and  $p$  is the prescribed pressure within the crack.

The given fracture geometry is discretized into elements – line segments in 2D and rectangular elements in 3D. Each of the DD elements of the discretized problem is assumed to send a set of stress influences to each of the other receiving elements in the mesh. These stress influences are determined by adding the integrated uniform stress components  $\sigma_{zz}^{l,\mu}$  and the integrated low frequency stress components  $\sigma_{zz}^{l,\mathcal{L}}$  at receiving points located at the centers of the receiving elements. Assembling all possible send–receive pairs of influences and storing them in a matrix  $C$ , we obtain the following discrete form of the above crack integral equation:

$$\sum_{n=1}^N C_{mn} w_n = p_m .$$

In order to represent arbitrary fracture fronts on a rectangular mesh in 3D without incurring any ‘staircasing’ errors, we make use of the concept of partially fractured tip elements introduced by Ryder and Napier (1985). This technique makes it possible to obtain a width profile that is as accurate as that obtained by using linear elements, or by using specialized square root tip elements.

## 7. Numerical results

In this section we provide some numerical results to illustrate the use of the UAS.

### 7.1. ASYMPTOTIC SOLUTION FOR A DD CLOSE TO AN INTERFACE

In this subsection we provide some results that demonstrate the performance of the UAS. In particular we consider the spectral coefficients associated with a square element whose size is 0.1 m and which just touches the bottom interface of a layer that is 0.4 m thick (see Figure 3).

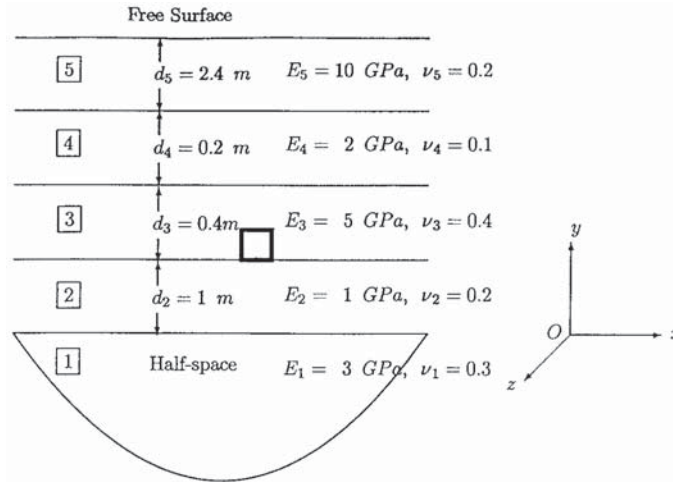


Figure 3. Geometry for UAS test problem.

We observe that relative positions of the layers and the size of the element are not drawn to scale in this figure.

In Figure 4 the spectral coefficients  $A_1^{4,Ps}(k)$ ,  $A_1^{4,Ps\mu}(k)$ , and  $A_1^{4,Ps\infty}(k)$  have all been plotted for comparison.  $A_1^{4,Ps}(k)$  represents the actual spectral coefficient that is associated with pseudo-layer 4 that is formed by inserting the false layer to model the source within the 3rd layer shown in Figure 3.  $A_1^{4,Ps\mu}(k)$  is the spectral coefficient obtained using the UAS, and  $A_1^{4,Ps\infty}(k)$  is the asymptotic solution that would be obtained if the medium were homogeneous having the same material properties as those of the so-called source layer indicated by the label 3 shown in Figure 3. The spectral coefficient  $A_1^{4,Ps\infty}(k)$  is the high frequency component that is typically subtracted out (see, for example, Pan, 1997; Lin and Keer, 1989; Wardle, 1980) in order to leave only the low frequency components that can be inverted and integrated numerically. We observe that there is a significant difference between the actual spectral coefficients  $A_1^{4,Ps}(k)$  for this problem and the homogeneous coefficients  $A_1^{4,Ps\infty}(k)$  for all but the very highest wavenumbers  $k \gtrsim 10^{2.5}$ . By contrast the actual spectral coefficients  $A_1^{4,Ps}(k)$  and the spectral coefficients derived from the UAS already show close agreement for wavenumbers  $k \approx 10^1$ . Although these two types of spectral coefficients are significantly different for a large portion of the low wavenumber spectrum shown in Figure 4 (note that the wavenumbers are plotted using a logarithmic scale), the contributions of the wavenumbers can be relatively easily integrated because they are associated with components whose spatial variations do not oscillate widely. In contrast, it would take considerable numerical resources to accurately integrate wavenumber components that are associated with functions which are oscillating rapidly in space such as those associated with  $k \gtrsim 10^2$ . Thus the UAS makes it possible to evaluate the influence of integrated, touching elements using relatively low order Gauss integration. Indeed, with the experiments performed, two-point Gauss integration was found to be sufficient for this purpose.

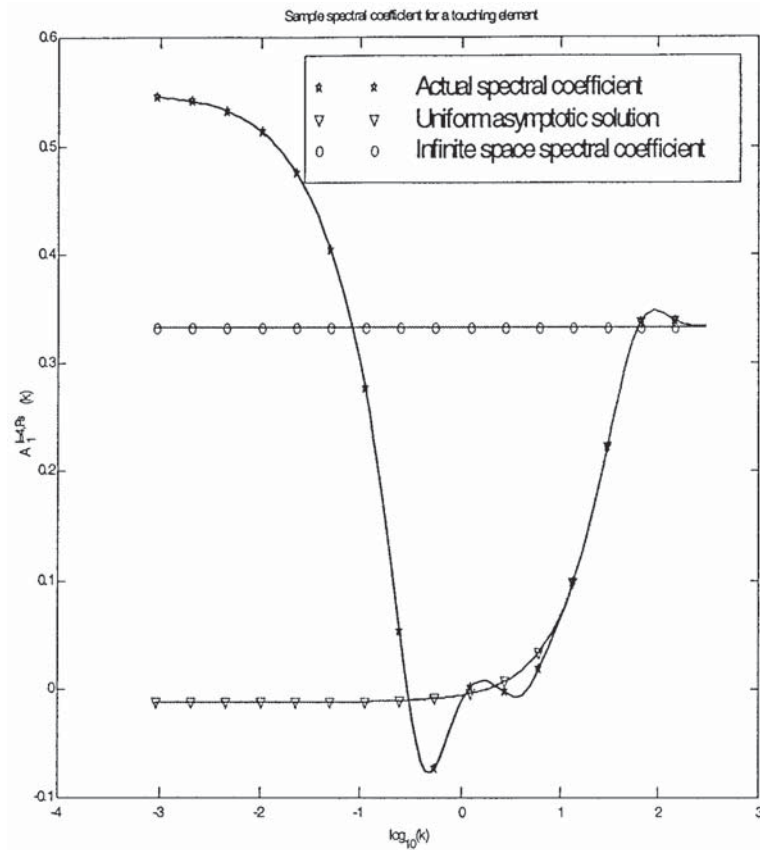


Figure 4. A sample spectral coefficient for an element that is touching an interface.

## 7.2. SOLUTION FOR A SINGLE DD TOUCHING INTERFACES

The first example involves calculating the stress profile for a single vertical DD in a 2D layered medium comprising four distinct layers (see Figure 5). The DD touches the two interfaces bounding three of the layers. This problem has been chosen so that it is possible to compare the stress influences due to a single DD obtained using the UAS procedure described above with those obtained using a boundary integral program DIGSMM (see Napier, 1998). A problem of any greater complexity would have exhausted the memory required by DIGSMM to solve the problem.

In the DIGSMM simulations, the constant strength DD solution in a layered material was obtained by discretizing the three interfaces between the layers and the free surface using piecewise linear DD elements. The solution to the DD problem was obtained by requiring that the displacements and tractions are continuous across the internal layer interfaces, while zero traction boundary conditions were applied at the free surface. In Figure 6 the spectral solution based on the UAS is compared with three sets of DIGSMM results, each corresponding to different discretizations with the available number of elements, by plotting the percentage differences between the DIGSMM solutions and the spectral solution. In the coarse DIGSMM mesh, 717 DD elements were used to represent the interfaces, the surface, and the single

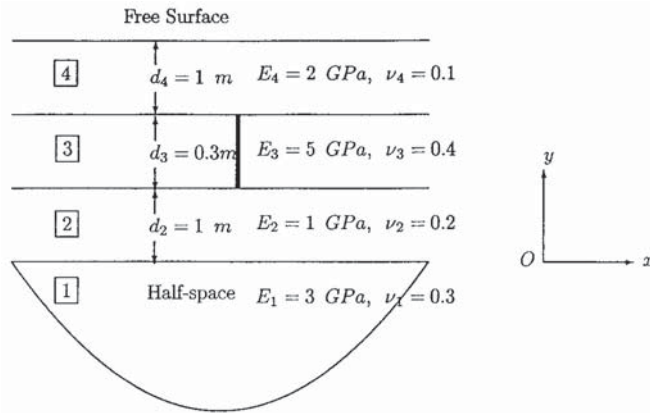


Figure 5. Geometry for problem to test the UAS using a DD that touches two interfaces.

vertical DD element itself. In this case the horizontal interfaces and the free surface were discretized to a distance of 15 m from the vertical DD, using a graded mesh. The spectral and DIGSMM solutions show good agreement in this case as can be seen from Figure 6. In order to assess whether the discrepancy is due to the spectral solution based on the UAS, or the discretization error in the DIGSMM solution, a second DIGSMM run was performed with a finer DD mesh. In the fine DD mesh 1,023 DD elements were used to discretize the same pieces of the interfaces but with a somewhat higher density of DD elements. It can be seen that the solution for the finer mesh has moved toward that of the spectral solution, particularly at those points close to the vertical DD edges. In order to determine the effect of the truncation of the layers in the DIGSMM model, another approximate solution was obtained in which the number of DD elements was increased to 1143 and the length of the discretized interfaces was extended to 38 m away from the vertical DD. In this case, there was no noticeable difference between the coarse solution and the extended solution in the benchmark points close to the vertical DD.

However, as the sample points are moved further from the vertical DD (see Figure 7), the fine solution and the coarse solution give results that differ noticeably from that of the spectral solution, while the extended solution shows much closer agreement with the spectral solution. This is due to the error made in the DIGSMM models when the interface discretization is terminated at a distance of 15 m from the vertical DD. The extended DIGSMM solution, in which the cut-off was 38 m, shows a much closer agreement with the spectral solution. The accuracy of the spectral solution in the far-field regime is dependent on accurate inversion and integration of the low wavenumber components  $\sigma_{ij}^{l,\ell}$ .

### 7.3. A VERTICAL CRACK TOUCHING AN INTERFACE

In this example we demonstrate the performance of the UAS by solving a problem in which a crack just touches an interface in a two layer elastic medium comprising a half-space onto which a 1 m layer of different modulus is bonded. This simple problem, containing only two layers, has been chosen to allow comparison with other simulators. The precise geometry and material properties for the problem are shown in Figure 8.

Two solutions for this problem were generated using ABAQUS (1998), one using 4,000 finite elements (FEs), and the other using 16,000 FEs. The width profiles which are associated

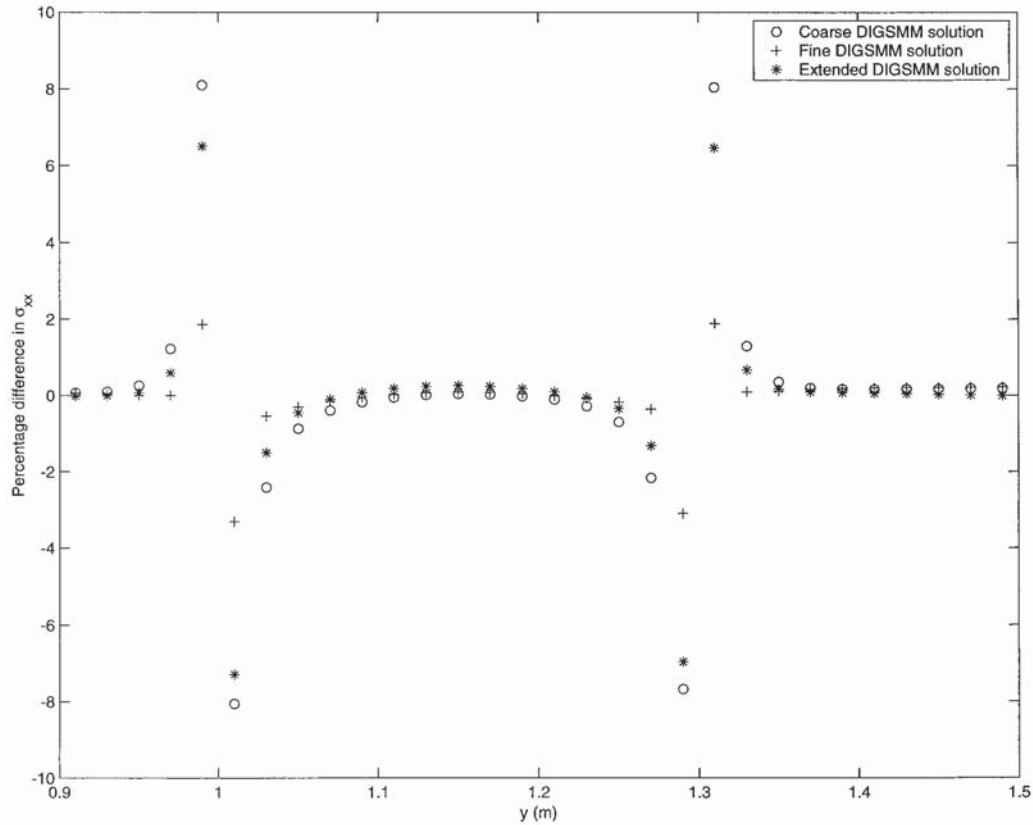


Figure 6. Percentage differences between FT solution and DIGSMM solutions.

with these solutions are plotted along a portion of the crack in Figure 9 using triangular and circular symbols respectively. A solution to this problem using 20 piecewise linear DD elements to model the crack as well as DD elements along the bonded interface and free surface was generated using DIGSMM (Napier, 1998) and the width profile for this solution is shown in Figure 9 using a dashed line. A solution using a bonded half-plane solution and 15 piecewise quadratic elements to model the crack itself as well as quadratic elements distributed along the free surface was generated using BHP (Selcuk, 1998), and the width profile is shown in Figure 9 using the square symbols. Finally, we generated two distinct spectral solutions exploiting the UASs described in this paper. Using MLAYER2D, a 2D spectral solution was determined involving 20 piecewise constant DD elements to model the crack. These elements are non-standard because they include special truncation correction terms (Ryder and Napier, 1985), which ensure very accurate width results. The influence functions for these elements were constructed using the 2D UAS given in Appendix C.2. Using MLAYER3D, a 3D spectral solution was determined involving 160 rectangular piecewise constant DD elements with truncation error correction. The rectangular elements had a large aspect ratio in order that the 3D model could approximate the 2D plane strain situation. The influence functions for these rectangular elements were constructed using the 3D UAS described in Appendix C.3.

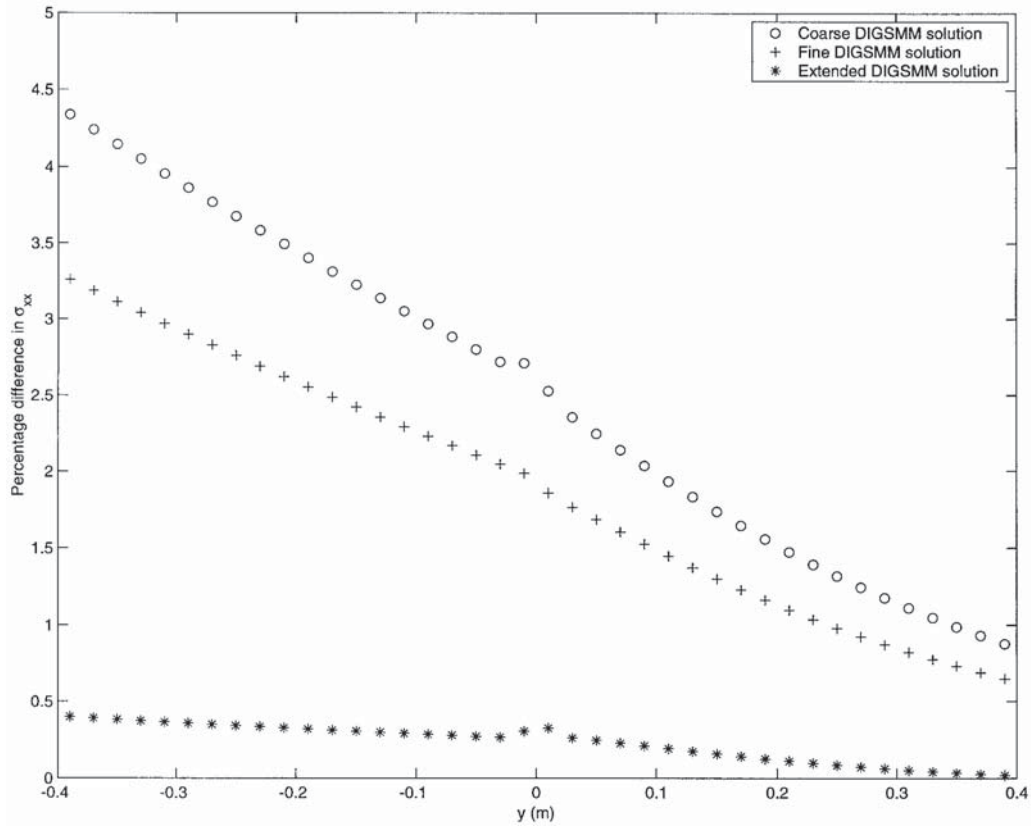


Figure 7. Percentage differences between FT solution and DIGSMM solutions for sample points remote from the DD.

Firstly we note that differences between the results shown in this plot have been emphasized by adjusting the ranges of the axes. There is in fact no more than a 0.6% difference between any of the solutions shown in this plot. We observe that the 4,000 element FE solution and the 20 element DIGSMM solution are fairly close to one another. When the FE model is refined to 16,000 elements the solution can be seen to move closer to the spectral solutions

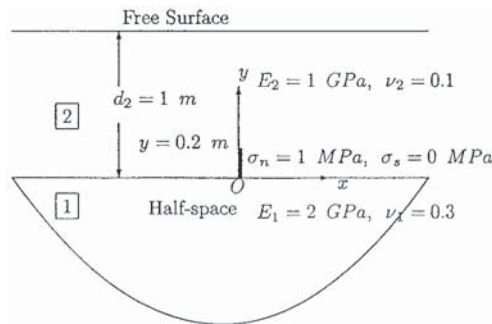


Figure 8. Geometry for problem in which a crack touches an interface.

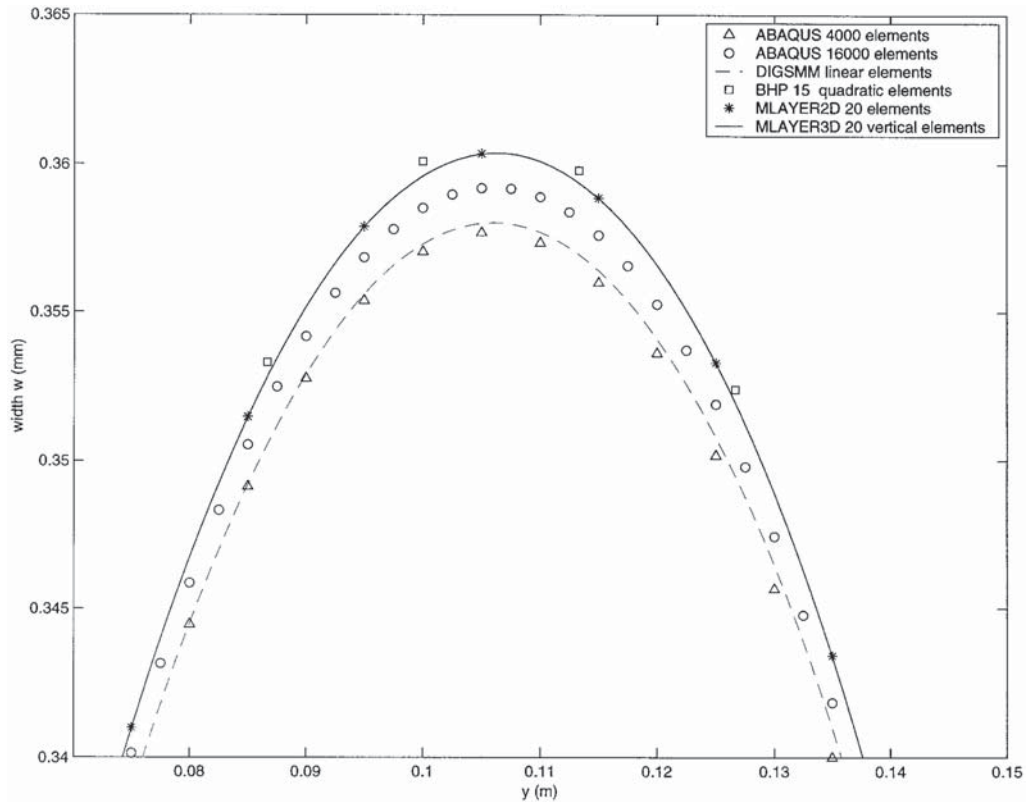


Figure 9. Width profiles for the pressurized crack problems using various algorithms.

and that given by the BHP solution. The two spectral solutions show very good agreement even through one is based on a 3D approximation to plane strain. Given the close agreement between the spectral solutions and the BHP solution (which is expected to give a very accurate result for this problem since the bonded half-plane part of the solution has been built into the solution explicitly) and the direction in which the FE solution moved with mesh refinement, it follows that the spectral solutions are highly accurate while the FE and DIGSMM models did not have enough degrees of freedom to give as accurate a result.

#### 7.3.1. Comparison of CPU times

To give an idea of the relative efficiency of the algorithms used in this problem, in Table 1 we list the CPU times in seconds for a dedicated 200 MHz Pentium processor. We observe that the more standard 2D finite element (ABAQUS) and boundary integral (DIGSMM) algorithms took substantially longer to compute the solutions to this problem in spite of the fact that the solutions were less accurate than the spectral method. The 2D spectral algorithm MLAYER2D is clearly highly efficient.

#### 7.4. A CRACK INTERSECTING TWO LAYERS

In this section we compare the numerical results for the case of a crack passing through the interface between two bonded half planes with some of the semi-analytic results provided

Table 1. Comparative CPU times for the crack touching an interface problem

Algorithm	Total no. of elts.	No. of elts. on crack	CPU time
ABAQUS (2D)	4000	40	175 s
DIGSMM (2D)	650	20 piecewise linear elements	147 s
MLAYER2D	20	20	0.17 s
MLAYER3D	160	20 vertical elements	78 s

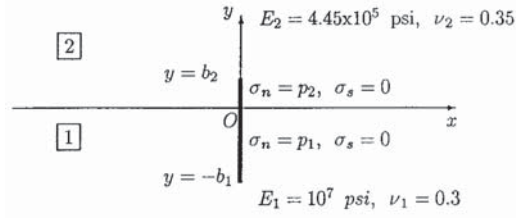


Figure 10. Geometry for problems in which a crack cuts through an interface.

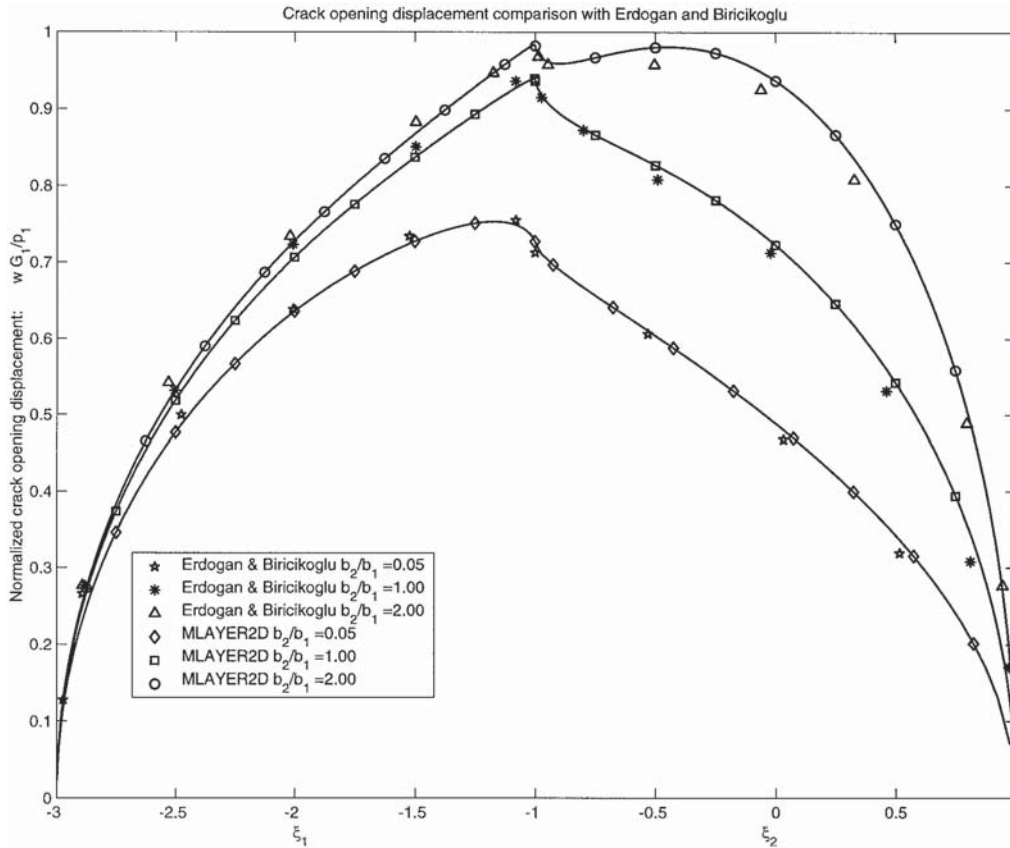


Figure 11. Crack opening displacement for crack subjected to constant stress  $p_1$  and  $p_2$ .

Table 2. Stress intensity factors determined using MLAYER2D and those given by Erdogan and Biricikoglu

$b_2/b_1$	MLAYER2D		Erdogan and Biricikoglu	
	$K_I(b_1)/(p_1\sqrt{l})$	$K_I(b_2)/(p_2\sqrt{l})$	$K_I(b_1)/(p_1\sqrt{l})$	$K_I(b_1)/(p_2\sqrt{l})$
0.05	1.4035	4.2268	1.4067	4.3607
1.00	1.0921	1.1586	1.0931	1.1787
2.00	0.9124	0.9676	0.9129	0.9770

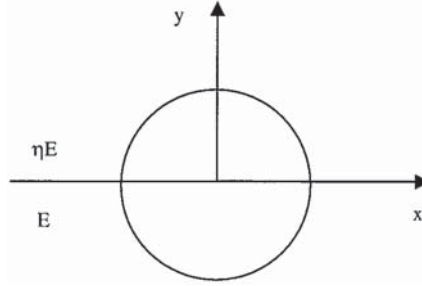


Figure 12. Geometry of a penny shaped crack centered on the interface between two different elastic media.

by Erdogan and Biricikoglu (1973). We consider a crack of length  $2l = b_1 + b_2$  to straddle the interface between two elastic half spaces with moduli:  $E_1 = 10^7$  psi,  $\nu_1 = 0.3$ , and  $E_2 = 4.45 \times 10^5$  psi,  $\nu_2 = 0.35$ . The  $b_1$  and  $b_2$  portions of the crack are loaded with constant pressures  $p_1$  and  $p_2$  respectively. In order to maintain continuity between the layers in a state of plane strain (Erdogan and Biricikoglu, 1973),  $p_1$  and  $p_2$  are related by:

$$\frac{1 - \nu_1^2}{E_1} p_1 = \frac{1 - \nu_2^2}{E_2} p_2.$$

In Figure 11 we plot, for comparison, the normalized crack opening displacements determined using MLAYER2D and those published in Erdogan and Biricikoglu (1973) (extracted from their paper by digitization). The normalized crack opening displacement is defined as  $wG_1/p_1$ . We observe that there is close agreement between the two sets of solutions.

In Table 2 we compare the stress intensity factors determined using MLAYER2D with those given by Erdogan and Biricikoglu. Erdogan and Biricikoglu (1973) define the stress intensity factor to be  $K_I(b_i) = \lim_{r_i \rightarrow 0} \sqrt{2r_i} \sigma_{xx}$ , where  $r_i = |b_i - y|$ . The stress intensity factors for the MLAYER2D results were obtained by expanding the width in terms of a two term asymptotic expansion:

$$w \underset{r \rightarrow 0}{\sim} c_0 r_0^{1/2} + c_1 r^{3/2} + O(r^{5/2}) \quad (7.1)$$

and using the coefficient of the leading term to determine  $K_I$ .

We observe that the stress intensity factors sampled at the tip of the  $b_1$  section of the crack differ by less than 0.1% between the two methods, while the stress intensity factors sampled at the tip of the  $b_2$  section of the crack differ by between 1% and 3%.

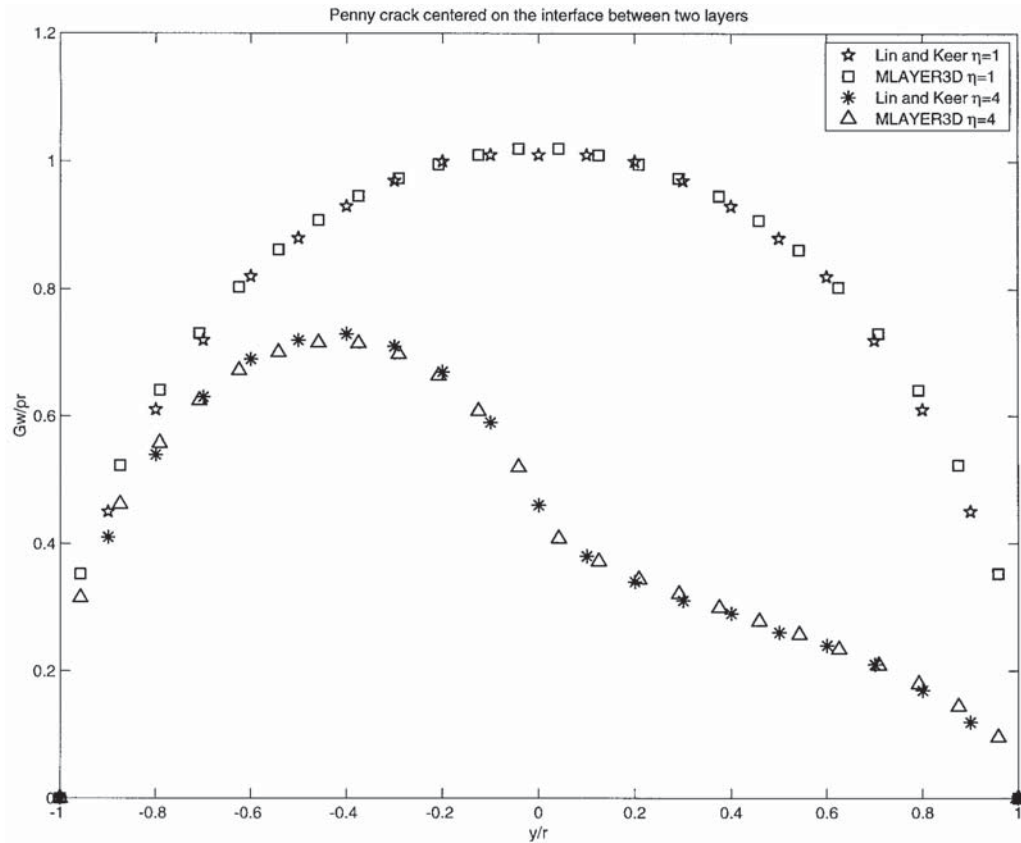


Figure 13. Normalized width profile for a penny shaped crack centered on the interface between two layers.

7.5. A PENNY SHAPED CRACK SPANNING TWO BONDED HALF SPACES

Lin and Keer (1989) have published results for the width of a penny shaped crack spanning a two-layer material (see Figure 3). Poisson’s ratio is assumed to be the same in both layers while the modulus contrast is given by a factor  $\eta$  as shown in Figure 12 and the penny crack is subjected to a constant pressure  $p$ .

In Figure 13 the normalized crack width  $Gw/pr$  is plotted against the normalized distance  $y/r$  along the vertical section through the crack centre. As can be seen there is a close agreement between the M-LAYER3D results and those published by Lin and Keer (extracted from their paper by digitization). The M-LAYER3D solution was generated using a parent mesh of 900 elements and required a total CPU time of 43 seconds on a 200 MHz PC.

7.6. A PENNY SHAPED CRACK BELOW THE INTERFACE BETWEEN TWO BONDED HALF SPACES

Kuo and Keer (1995) have published stress intensity results for a penny shaped crack located near to the interface between two bonded layers. We consider the case of a penny shaped crack of radius  $c$  which is located a distance  $h = 1.2c$  below the interface between the two layers as shown in Figure 14. The lower and upper layers are assigned elastic moduli  $E_1, \nu_1$  and  $E_2, \nu_2$

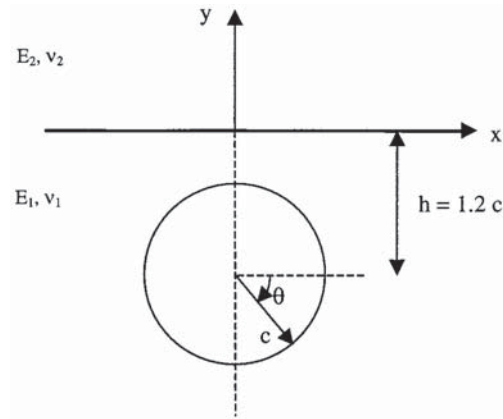


Figure 14. Location of a penny shaped crack just below the interface between two bonded half spaces.

respectively. For the purposes of the comparison, the same Poisson's ratio  $\nu_1 = 0.3 = \nu_2$  is assigned to both of the layers, the ratio of the corresponding shear moduli of the two layers,  $\Gamma = G_2/G_1$ , is varied, and the penny crack is subjected to a constant pressure  $p$ .

In Figure 15 we plot the normalized stress intensity factor  $K_I/(p\sqrt{\pi c})$  against the angle  $\theta$  as defined in Figure 14. The Kuo and Keer results that have been plotted in Figure 15 have been extracted from their paper by digitization. They define the stress intensity factor to be  $K_I(\theta) = \lim_{r \rightarrow 0} \sqrt{2\pi r} \sigma_{zz}(r, \theta)$ , where  $r$  is the distance measured from the tip of the crack (we note that this definition of the stress intensity factor differs from that used by Erdogan and Biricikoglu (1973) by a factor of  $\sqrt{\pi}$ ). The stress intensity factor for the MLAYER3D results are determined by sampling the width profile a distance  $r$  from the crack tip by making use of a bi-quadratic interpolation on a local 3 by 3 patch of piecewise constant DD elements, which are chosen so that the sample point falls within the central element of the patch. Making use of two such sampled widths, both on the same radial line defined by  $\theta = \text{constant}$ , the asymptotic expansion (7.1) is then used to determine the stress intensity factor by making use of the leading order coefficient  $c_0$  according to:

$$K_I = \sqrt{\frac{\pi}{2}} \frac{G}{2(1-\nu)} c_0,$$

where  $G$  and  $\nu$  are the shear modulus and Poisson's ratio of the layer in which the tip point falls.

For the case of a homogeneous material, the stress intensity factor for a penny crack (Kuo and Keer, 1995), loaded by a constant pressure  $p$ , is given by:

$$\frac{K_I}{p\sqrt{\pi c}} = \frac{\pi}{2} \approx 0.6366.$$

We observe that for the homogeneous case,  $\Gamma = 1$ , the MLAYER3D results (depicted by the  $\star$  symbols without the line) shows a close agreement with the exact solution, which is represented by the solid horizontal line. The minor fluctuations in the MLAYER3D result is a consequence of the interpolation errors incurred in the sampling process. We also note that the Kuo and Keer result is larger than the exact solution by a constant amount of 0.0086, which

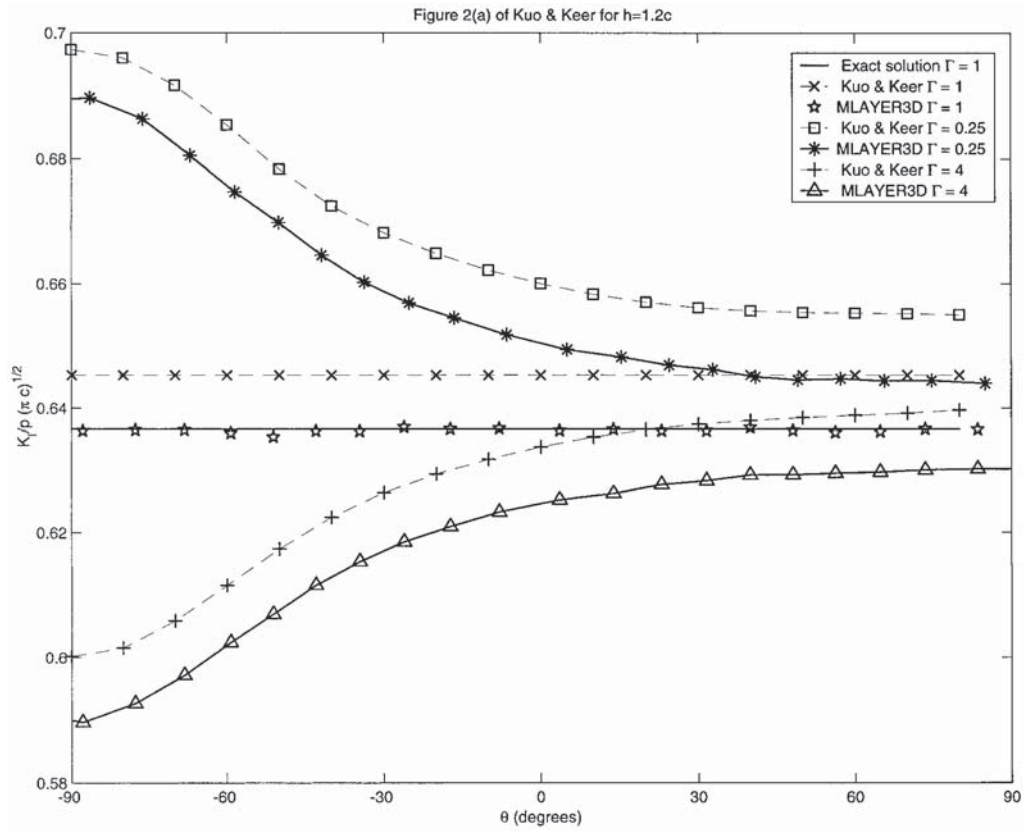


Figure 15. Variation of the normalized stress intensity factor  $K_I/(p\sqrt{\pi c})$  along the perimeter of the penny crack with the angle  $\theta$ .

represents an error of 1.4% and is probably due to the truncation error of the discretization procedure that they used to determine their results. We observe that for the cases  $\Gamma \neq 1$ , the M-LAYER3D results and the Kuo and Keer results show the same trend, except that, as was the case in the homogeneous situation, the Kuo and Keer result is consistently larger than the M-LAYER3D result by a constant factor. Indeed, if the constant amount of 0.0086 is subtracted from all the Kuo and Keer results, then their results closely match the M-LAYER3D and exact results.

In Table 3 the M-LAYER3D stress intensity factors are presented for various refinements of the parent mesh, which circumscribes the penny crack region. We observe that for the case  $\Gamma = 1$  the approximate stress intensity approaches the exact value at a rate of  $O(\Delta x^3)$  as the size  $\Delta x$  of the square DD elements is refined. There is a similar trend in the stress intensity factors for the values of  $\Gamma$  as the mesh is refined. The CPU times quoted are for a 200 MHz Pentium computer.

Table 3. MLAYER3D stress intensity factors for various parent meshes

	$\delta = 90^\circ$			$\theta = 90^\circ$		
	$24 \times 24$	$48 \times 48$	$96 \times 96$	$24 \times 24$	$48 \times 48$	$96 \times 96$
$N \times N$	$24 \times 24$	$48 \times 48$	$96 \times 96$	$24 \times 24$	$48 \times 48$	$96 \times 96$
$\Gamma = 0.25$	0.6882	0.6893	0.6898	0.6525	0.6453	0.6438
$\Gamma = 0.25$	0.6454	0.6381	0.6365	0.6455	0.6381	0.6365
$\Gamma = 0.25$	0.6084	0.5927	0.5885	0.6392	0.6313	0.6297
CPU time	47.5 s	197.5 s	1293 s	47.5 s	197.5 s	1293 s

## 8. Conclusions

In this paper we have presented UASs that make it possible to efficiently model cracks that touch or intersect interfaces between layered elastic media. When modeling cracks that touch or intersect interfaces, the source DDs introduce high wavenumber components into the spectral solution to multilayer problems that cannot be treated numerically. The UASs enable one to subtract out the high wavenumber components from the spectral solution for multiple layer elastic problems leaving only low wavenumber components that need to be inverted numerically. Since these low wavenumber components are associated with modes whose spatial variation is moderate, they can be inverted and integrated with low order Gauss integration. In this paper we have described the process by which the UASs can be constructed for 2D and 3D layered elastic media. The process of analytic integration of these singular solutions is also described.

In this paper we provide numerical evidence that demonstrates that the UAS captures a substantial portion of the high wavenumber spectrum which reduces the computational burden of numerical inversion and integration of the spectral solutions. We also provide a number of numerical examples in which the accuracy and speed of the spectral method is compared with that of the finite element method and a boundary integral formulation for multiple elastic layers. The spectral solution was shown to be more accurate compared to the other methods while using substantially less computer resources in terms of memory and computational time. We demonstrated that the MLAYER2D crack widths and stress intensity factors compared well with published results for a line crack that intersects two bonded half planes. We demonstrated that the MLAYER3D fracture widths and stress intensity factors for a penny shaped crack in two bonded half spaces show close agreement with results published in the literature.

## Acknowledgements

The authors wish to thank Schlumberger for permission to publish this work. In addition, the authors wish to thank Professor S.L. Crouch, Dr J.A.L. Napier, and Dr P. Papanastasiou for useful discussions, and for running some of the test models.

## Appendix A. Definition of the FT

Let  $g(x, z) \in L^1(R^2)$  then we define the double FT of  $g(x, z)$  to be

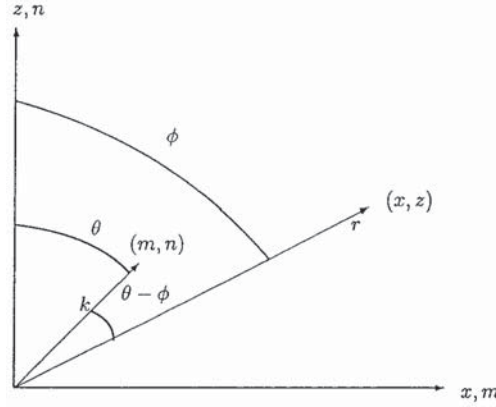


Figure B1. Polar coordinates for the FT inversion.

$$\hat{g}(m, n) = \int_{-\infty}^{\infty} \int_{-\infty}^{\infty} e^{i(mx+nz)} g(x, z) dx dz \quad (\text{A.1})$$

and the corresponding inversion formula is:

$$g(x, z) = \frac{1}{(2\pi)^2} \int_{-\infty}^{\infty} \int_{-\infty}^{\infty} e^{-i(mx+nz)} \hat{g}(m, n) dm dn . \quad (\text{A.2})$$

### Appendix B. Inversion of the 3D kernels

We now outline the procedure that is used to invert the double FT by first converting to polar coordinates in order to rewrite the FT in the form of a Hankel transform. The FT of the horizontal stress component  $\hat{\sigma}_{zz}$  due to a point vertical DD of unit strength located a distance  $\eta$  from the center of the sending element (see Figure C1) is of the form:

$$\begin{aligned} k\hat{\sigma}_{zz} = & f n^2 \left\{ A_1^{Ps\mu}(k) + A_1^{As\mu}(k) \frac{m^2}{k^2} \right\} e^{-ky'} + \\ & (-l_6 n^2 - l_7 m^2 + f n^2 k y') \left\{ A_2^{Ps\mu}(k) + A_2^{As\mu}(k) \frac{m^2}{k^2} \right\} e^{-ky'} - f \frac{m^2 n^2}{k^2} A_5^{At\mu} e^{-ky'} - \\ & f n^2 \left\{ A_3^{Ps\mu}(k) + A_3^{As\mu}(k) \frac{m^2}{k^2} \right\} e^{-ky'} + \\ & (-l_6 n^2 - l_7 m^2 - f n^2 k y') \left\{ A_4^{Ps\mu}(k) + A_4^{As\mu}(k) \frac{m^2}{k^2} \right\} e^{-ky'} - f \frac{m^2 n^2}{k^2} A_6^{At\mu} e^{-ky'} , \end{aligned} \quad (\text{B.1})$$

where the spectral coefficients  $A_j^\mu(k)$  are those for the uniform asymptotic approximation defined in (4.2), (4.7), and (4.12). The detailed coefficients  $A_j^\mu(k)$  and constants  $f$ ,  $l_6$ , and  $l_7$  will vary depending on which of the four layers indicated in Figure 2 the receiving point falls in.

Applying the inverse FT defined in (A.2) we obtain

$$\sigma_{zz}(x, z) = \frac{1}{(2\pi)^2} \int_{-\infty}^{\infty} \int_{-\infty}^{\infty} e^{-i(mx+nz)} \hat{\sigma}_{zz}(m, n) \, dm \, dn . \quad (\text{B.2})$$

We now express the integration variables  $m$  and  $n$  in (B.2) in terms of polar coordinates  $(k, \theta)$  in which  $m = k \sin \theta$  and  $n = k \cos \theta$ . We also express  $x$  and  $z$  in terms of the polar coordinates  $(r, \phi)$  so that  $x = r \sin \phi$  and  $z = r \cos \phi$  (see Figure B1).

In terms of these new variables

$$mx + nz = kr \cos(\theta - \phi) ,$$

so that (B.2) can be written in the form:

$$\sigma_{zz}(r \sin \phi, r \cos \phi) = \frac{1}{(2\pi)^2} \int_{-\infty}^{\infty} \int_{-\pi}^{\pi} e^{-ikr \cos(\theta-\phi)} \hat{\sigma}_{zz}(k \sin \theta, k \cos \theta) \, d\theta \, dk . \quad (\text{B.3})$$

By introducing the notation:

$$K_{pq}(k; r, \phi) = \frac{1}{2\pi} \int_{-\pi}^{\pi} e^{-ikr \cos(\theta-\phi)} \cos^p \theta \sin^q \theta \, d\theta , \quad (\text{B.4})$$

we can write the terms in  $\hat{\sigma}_{zz}(k \sin \theta, k \cos \theta)$  as a linear combination of integrals of the following form:

$$I_{spq} = \frac{1}{2\pi} \int_0^{\infty} e^{-ky'} A_j(k) k^s K_{pq} \, dk . \quad (\text{B.5})$$

Now making use of the identity (see Olver, 1974):

$$J_n(\rho) = \frac{1}{2\pi} \int_{-\pi}^{\pi} e^{-in\theta} e^{i\rho \sin \theta} \, d\theta , \quad (\text{B.6})$$

where  $J_n$  is the  $n$ -th order Bessel function, it is possible to represent the integrals  $K_{pq}$  in the form:

$$K_{pq} = \sum_{j=0}^{p+q} \left( \sum_{i=0}^j b_i \left( \frac{z}{r} \right)^{2i} \right) J_{2j}(kr) . \quad (\text{B.7})$$

Thus by making use of (B.3–B.7) it is possible to invert  $\hat{\sigma}_{zz}$  by evaluating Hankel transforms of the form:

$$H_n(r) = \int_0^{\infty} h(k; x, y, r) J_n(kr) \, dk .$$

## Appendix C. Integrated kernels

### C.1. PROCEDURE FOR VERTICAL INTEGRATION

In this appendix we describe the process of determining the approximate spatial stress influences due to a vertical DD element that lies in the middle layer of a pack of three different



and subsequent integration process, consider a point vertical DD to be located a distance  $\eta$  from center of the element. On this horizon, we have inserted a dashed line, that represents the pseudo layer that is needed to represent the interface across which we need to apply the appropriate jump conditions to obtain a point vertical DD. In Figure C.1, the receiving point is represented by the open circle just below the top interface of the middle layer. The distance from the point DD to the receiving point is denoted by  $y'$ , while the distance from the center of the vertical DD element is denoted by  $y = y' + \eta$ . Let  $h_U$  and  $h_L$  denote the distance from the point vertical DD to the upper and lower interfaces of the middle layer respectively, while  $h_U^0$  and  $h_L^0$  represent the distances from the center of the sending element to the upper and lower interfaces of the middle layer respectively. Let  $\Delta y_U$  and  $\Delta y_L$  denote the distances between the receiving point and the upper and lower interfaces of the middle layer respectively. Let  $y_{IU}$  and  $y_{IL}$  denote the distances from the centers of the upper and lower image elements to the receiving point.

The distances defined above are related in the following way:

*Lower image distances*

$$\begin{aligned} \Delta y_L = h_L^0 + y, \quad y_{IL} = 2h_L^0 + y, \quad y' = 2\Delta y_L - (y_{IL} + \eta), \quad h_L = h_L^0 + \eta, \\ h_L = \Delta y_L - y', \quad h_L = (y_{IL} + \eta) - \Delta y_L, \quad 2h_L + y' = y_{IL} + \eta. \end{aligned} \quad (\text{C.1})$$

*Upper image distances*

$$\begin{aligned} \Delta y_U = h_U^0 - y, \quad y_{IU} = 2h_U^0 - y, \quad y' = (y_{IU} - \eta) - 2\Delta y_U, \quad h_U = h_U^0 - \eta, \\ h_U = \Delta y_U + y', \quad h_U = (y_{IU} - \eta) - \Delta y_U, \quad 2h_U - y' = y_{IU} - \eta. \end{aligned} \quad (\text{C.2})$$

## C.2. INTEGRATED 2D KERNELS

Substituting the expressions for the spectral coefficients  $A_j^{l,\mu}(k)$  and in turn the expressions for the functions  $g_j^U(k)$  and  $g_j^L(k)$  in terms of the spectral constants  $\alpha_j^i$ ,  $c_0^L$ ,  $c_0^U$ ,  $c_3$ , and  $c_4$ ; inverting each of the resulting terms of the form  $k^p e^{-k|y|}$  using (A.2); and integrating the point DDs over the length  $2a$  of the element, we obtain the following expression for the horizontal stress  $\sigma_{xx}(x, y)$  due to a constant unit vertical DD element:

$$\begin{aligned} h_U^0 < y \\ \sigma_{xx}^\mu = f^3 \{ \alpha_0^{1L} \tilde{J}_{100}^L + \alpha_1^{1L} \tilde{J}_{201}^L + \alpha_2^{1L} \tilde{J}_{302}^L + \alpha_0^{0U} J_{100} + \alpha_1^{0U} J_{201}^U \} \\ - l_6^3 \{ \alpha_0^{2L} \tilde{J}_{100}^L + \alpha_1^{2L} \tilde{J}_{201}^L + c_0^U J_{100} \} \\ + f^3 \{ \alpha_0^{2L} \tilde{J}_{210}^L + \alpha_1^{2L} \tilde{J}_{311}^L + c_0^U J_{210} \} \end{aligned} \quad (\text{C.3})$$

$$\begin{aligned} -h_L^0 < y < h_U^0 \\ \sigma_{xx}^\mu = f^2 \{ \alpha_0^{1L} \tilde{J}_{100}^L + \alpha_1^{1L} \tilde{J}_{201}^L + \alpha_2^{1L} \tilde{J}_{302}^L \} + f^2 \{ \alpha_0^{2L} \tilde{J}_{210}^L + \alpha_1^{2L} \tilde{J}_{311}^L \} \\ - l_6^2 \{ \alpha_0^{2L} \tilde{J}_{100}^L + \alpha_1^{2L} \tilde{J}_{201}^L \} - f^2 \{ \alpha_0^{1U} \tilde{J}_{100}^L + \alpha_1^{1U} \tilde{J}_{201}^L + \alpha_2^{1U} \tilde{J}_{302}^L \} \\ - f^2 \{ \alpha_0^{2U} \tilde{J}_{210}^L + \alpha_1^{2U} \tilde{J}_{311}^L \} - l_6^2 \{ \alpha_0^{2U} \tilde{J}_{100}^U + \alpha_1^{2U} \tilde{J}_{201}^U \} + \\ - f^2 c_3 J_{100} + c_4 (f^2 J_{210} - l_6^2 J_{100}). \end{aligned} \quad (\text{C.4})$$

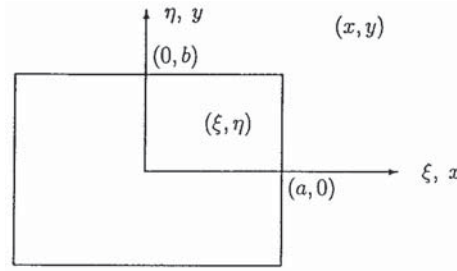


Figure C2. Integration of point influences over a rectangle.

$$\begin{aligned}
 y < h_U^0 \\
 \sigma_{xx}^\mu = & -f^1 \{ \alpha_0^{1U} \tilde{J}_{100}^U + \alpha_1^{1U} \tilde{J}_{201}^U + \alpha_2^{1U} \tilde{J}_{302}^U + \alpha_0^{0L} J_{100}^L + \alpha_1^{0L} J_{201}^L \} \\
 & - l_6^1 \{ \alpha_0^{2U} \tilde{J}_{100}^U + \alpha_1^{2U} \tilde{J}_{201}^U + c_0^L J_{100} \} \\
 & - f^1 \{ \alpha_0^{2U} \tilde{J}_{210}^U + \alpha_1^{2U} \tilde{J}_{311}^U - c_0^L J_{210} \}.
 \end{aligned} \tag{C.5}$$

Here the integrals  $J_{lmn}^{U/L}$  are defined as follows:

$$\begin{aligned}
 J_{pmn}^L &= \int_{y-a}^{y+a} I_p(x', y') \cdot (y')^m h_L^n dy' \\
 &= \int_{y-a}^{y+a} I_p(x', y') \cdot (y')^m (\Delta y_L - y')^n dy'
 \end{aligned} \tag{C.6}$$

$$\begin{aligned}
 J_{pmn}^U &= \int_{y-a}^{y+a} I_p(x', y') \cdot (y')^m h_U^n dy' \\
 &= \int_{y-a}^{y+a} I_p(x', y') \cdot (y')^m (\Delta y_U - y')^n dy'
 \end{aligned} \tag{C.7}$$

while the integrals associated with the image elements are defined as follows:

$$\begin{aligned}
 \tilde{J}_{pmn}^L &= \int_{y-a}^{y+a} I_p(x', 2h_L + y') \cdot (y')^m h_L^n dy' \\
 &= \int_{-a}^a I_p(x', y_{IL} + \eta) [2\Delta y_L - (y_{IL} + \eta)]^m [(y_{IL} + \eta) - \Delta y_L]^n d\eta,
 \end{aligned} \tag{C.8}$$

$$\begin{aligned}
 \tilde{J}_{pmn}^U &= \int_{y-a}^{y+a} I_p(x', 2h_U - y') \cdot (y')^m h_U^n dy' \\
 &= \int_{-a}^a I_p(x', y_{IU} + \eta) \cdot [(y_{IU} - \eta) - 2\Delta y_U]^m [(y_{IU} - \eta) - \Delta y_U]^n d\eta.
 \end{aligned} \tag{C.9}$$

Here we have made use of the image distances defined in (C.1) and (C.2).

#### INTEGRATED 3D KERNELS

To integrate the 3D point DD kernels given in (B.3) over a rectangular element as shown in Figure C2 the procedure is similar to that used in 2D in which the integrals (C.6)–(C.9) are replaced by integrals of the form:

$$I_{jls}^{pq,U}(y_{IU}) = \int_{x-a}^{x+a} \int_{y-b}^{y+b} (h_U)^l(y')^s \left\{ \int_0^\infty e^{-k(2h_U-y')} k^j K_{pq}(k, x') dk \right\} dx' dy' \quad (C.10)$$

$$= \int_{x-a}^{x+a} \int_{y_{IU}-b}^{y_{IU}+b} (\bar{y} - \Delta y_U)^l (\bar{y} - 2\Delta y_U)^s \left\{ \int_0^\infty e^{-k\bar{y}} k^j K_{pq}(k, x') dk \right\} dx' d\bar{y},$$

$$I_{jls}^{pq,L}(y_{IL}) = \int_{x-a}^{x+a} \int_{y-b}^{y+b} (h_L)^l(y')^s \left\{ \int_0^\infty e^{-k(2h_L+y')} k^j K_{pq}(k, x') dk \right\} dx' dy' \quad (C.11)$$

$$= \int_{x-a}^{x+a} \int_{y_{IL}-b}^{y_{IL}+b} (\bar{y} - \Delta y_L)^l (2\Delta y_L - \bar{y})^s \left\{ \int_0^\infty e^{-k\bar{y}} k^j K_{pq}(k, x') dk \right\} dx' d\bar{y},$$

$$I_{jls}^{pq}(y) = \int_{x-a}^{x+a} \int_{y-b}^{y+b} (h_U)^l(y')^s \left\{ \int_0^\infty e^{-k|y'|} k^j K_{pq}(k, x') dk \right\} dx' dy', \quad (C.12)$$

where the image distances defined in (C.1) and (C.2) have been used to simplify the evaluation of the integrals in (C.10)–(C.12). We only consider normal stress components that are evaluated in the plane of the vertical DD so that  $z = 0$  and  $r = |x|$ .

## References

- ABAQUS, HKS, Rhode Island, 1998.
- Bender, C.M. and Orszag, S.A. (1978). *Advanced Mathematical Methods for Scientists and Engineers* McGraw-Hill, New York.
- Buffler, H. (1961). Der Spannungszustand in einem geschichteten Körper bei axialsymmetrischer Belastung. *Ingenieur-archiv* **30**, no 6, 417–430.
- Buffler, H. (1962). Die Bestimmung des Spannungs und Verschiebungszustandes eines geschichteten Körperes mit Hilfe von Übertragungsmatrizen. *Ingenieur-archiv* **31**, no 1, 229–240.
- Buffler, H. (1971). Theory of elasticity of a multilayered medium. *Journal of Elasticity* **1**, no 2.
- Crouch, S.L. (1998). Personal communication.
- Crouch, S.L. and Starfield, A.M. (1990). *Boundary Element Methods in Solid Mechanics*, Unwin Hyman, London.
- Erdogan, F. and Biricikoglu (1973). Two bonded half planes with a crack going through the interface. *International Journal of Engineering Science* **11**, 745–766.
- Gilbert, F. and Backus, G.E. (1966). Propagator matrices in elastic wave and vibration problems. *Geophysics* **31**, 326–332.
- Kennet, B.L.N. (1983). *Seismic Wave Propagation in Stratified Media*, Cambridge University Press, Cambridge.
- Kuo, C.H. and Keer, L.M. (1995). Three-dimensional analysis of cracking in a multilayered composite, *ASME Journal of Applied Mechanics* **62**, 273–281.
- Lin, W. and Keer, L.M. (1989). Analysis of a vertical crack in a multilayered medium. *ASME Journal of Applied Mechanics* **56**, 63–69.
- Lin, W. and Keer, L.M. (1989). Three-dimensional analysis of cracks in layered transversely isotropic media. *Proceedings Royal Society London A*, **424**, 307–322.
- Linkov, A. and Filippov, N. (1991). Difference equations approach to the analysis of layered systems. *Meccanica* **26**, 195–209.
- Napier, J.A.L. (1998). Personal communication.
- Olver, F.W.J. (1974). *Asymptotics and Special Functions*, Academic Press Inc., New York.
- Pan, E. (1997). Static Green's functions in multilayered half spaces, *Applied Mathematical Modelling* **21**, 509–521.
- Peirce, A.P. and Siebrits, E. (2001). The scaled flexibility matrix method for the efficient solution of boundary value problems in 2D and 3D layered elastic media. *Computer Methods in Applied Mechanics and Engineering* (to appear).
- Ryder, J.A. and Napier, J.A.L. (1985). Error analysis and design of a large-scale tabular mining stress analyzer, *Proceedings 5th International Conference of Numerical Methods in Geomechanics*, Nagoya, 1549–1555.

- Selcuk, S. (1998). Personal communication via Crouch, S.L.
- Singh, S.J. (1970). Static deformation of a multilayered half-space by internal sources. *Journal of Geophysical Research* **75**,3257–3263.
- Singh, S.J. (1986). Static deformation of a transversely isotropic multilayered half-space by surface loads. *Physics of the Earth and Planetary Interiors* **42**, 263–273.
- Sneddon, I.N. (1995). *Fourier Transforms*, Dover, New York.
- Thompson, W.T. (1950). Transmission of elastic waves through a stratified medium, *Journal of Applied Physics* **21**, 89–93.
- Wallace, P.R. (1984). *Mathematical Analysis of Physical Problems*, Dover, New York.
- Wardle, L.J. (1980). Stress analysis of multilayered anisotropic elastic systems subject to rectangular loads, CSIRO Institute of Earth Resources, *Division of Applied Geomechanics, Technical Paper* **33**, Australia.